The
University
Of
Sheffield.

Department
Of
Mechanical
Engineering

MEng Mechanical Engineering

Reduction of the Ground Vibrations Induced By High-Speed Trains by Means of Isolations

Zhan **ZHANG**

August, 2018

Supervisor: Dr. Inna Gitman

Thesis submitted to the University of Sheffield in partial fulfilment of the requirements for the degree of Master of Engineering

SUMMARY

With the development in technology, the substantial expansion of the High-Speed Train (HST) has shown an unprecedented scale over the world and up till now, it is still ongoing. Despite the general benefits that it brings to the economy and social regional developments, the ground-borne vibrations induced by the passage of high-speed trains has been documented as an serious issue as it causes nuisance to many. In addition, the vital frequency range was found to be between 1 and 80 Hz by several national and international standards. Inspired by the band gap phenomena, in this contribution, a proposal of sub-grade filled with heterogenous materials, implemented on the ground close to the rail tracks, has been considered as a potential strategy to mitigate the propagation of elastic waves being transmitting over the soil. Through the gradient elasticity theory, the potential heterogenous periodic materials were selected as concrete and foam. The corresponding stop band frequency value was predicted to be less than 40Hz. A one-dimensional numerically model was then performed in order to demonstrate the response of the structure under the dynamic conditions and, at the same time, to verify the existence of the stop band frequency that was predicted by the gradient theory. The study was extended to investigate the influence of quasi-randomness in geometry on the overall responses of the structure. Results showed the responses of the model decayed with a higher rate but the position of the first stop band frequency remained unchanged. In conclusion, the contribution has initiated a possible solution of deploying heterogeneous material in order to isolate the ground-borne vibrations. Future research are required to explore this work both numerically and experimentally.

CONTENTS

List of Figures

List of Tables

NOMENCLATURE

The next list describes several symbols that will be later used within the body of the document.

Acronym

BEM   Boundary Element Method

FDTD   Finite Difference Time Domain

FEM   Finite Element Method

HST   High-Speed Train

PML   Perfectly Matched Layer

RVE   Representative Volume Element

Greek Symbols

α volume fraction

$\alpha(s)$ nonlocal weight function for stress tensor

β_ρ contrast ratio of mass density

β_E contrast ratio of Young's modulus

Δ constant linear change in quantity

δ rate of change in quantity

γ dimensionless coefficient with regards to the impedance of periodic material

λ wave length

Ω volume domain of the structure

ω angular frequency of wave propagation

Π potential energy

ρ	mass density of the material
σ	stress
σ_{ij}	stress tensor for continuum material
ε	strain
ε_{kl}	strain tensor for continuum material

Roman Symbols

B	strain matrix
d	vector of nodal displacements
F	body force matrix
K	stiffness matrix
L	modified derivative operator
N	matrix of shape function
u	matrix of continuous displacement
v	vector of velocity
A_c	cross-sectional area
b_i	body force components
C_{ijkl}	constitutive matrix consists of the fourth-order tensors
E	Young's modulus or elastic modulus
F	applied force
f	wave frequency (Hz)
k	wave number, $k = \omega/V$, where V is the wave speed
k_s	spring constant
L	length of representative volume element
l	length-scale parameter

l_c	length of unit periodic cell
L_e	length between two nodes in one element
p	external loading
T	kinetic energy
t	time
T_λ	time period for one wave length
T_c	transmission of coefficient
U	strain energy
u	displacement
V	wave speed
v	velocity
W	work done by external load
x	position on x-axis
Z	elastic wave impedance

Superscripts

c	classical theory
g	gradient theory

Subscripts

$1, 2$	material number
dyn	dynamic
e	effective quantity
i, j, k, l	notion of degree of freedom
n	step number
p	P-wave (compressional wave)

s	S-wave (shear wave)
$stat$	static
$heter$	heterogeneous material
$homo$	homogeneous material

Other Symbols

$\ddot{u}$	acceleration component
Δu	elongation of the spring from its equilibrium state
$\dot{u}$	velocity component
$\dot{\mathbf{u}}$	vector of nodal degree-of-freedom velocities
$\frac{\partial u_k}{\partial x_l}, \frac{\partial u_l}{\partial x_k}$	strain components in classical theory

ACKNOWLEDGEMENT

1 INTRODUCTION

In this section, the background information of the project was presented in order to demonstrate the severity of the induced ground-borne vibrations from the passage of high-speed trains and to initiate motivation for solving such issues. The section was comprised of a holistic literature review with regards to the elements that paved the way to the present concerns in this project and, potentially, to the research in the future. They included vibration generation, wave propagation, damaging frequency range, numerical soil modelling, numerical mitigation methods, and stop band phenomena.

1.1 Background

With the acceleration of innovation in technology, the substantial expansion of the High-Speed Trains (HST) has shown an unprecedented scale over the world and yet, it is still ongoing. The infrastructure is in the view of establishing a high-performance transportation in dense population areas [4].

Despite general acknowledgement of HST's overwhelming superiority in economic and social regional development, there has been a number of imperative considerations taking account into the negative side-effects of the passenger trains as a result of continuously increasing in speed. Abnormal high-vibrations at the interface of wheels and tracks were observed when the train was operating at high speed, which were then transmitted to the soil through the tracks [5].

These vibrations will become excessive when the train speed is high enough to resonate the tracks, thus resulting in detrimental effects both physically and psychologically to humans in the nearby community [6]; at the same time, it will damage the integrity of the structures in the vicinity of external vibration sources by imposing dynamic loads to go beyond material's enduring limit (cracks due to material fatigue are often the first visible defects) [7]. On the other hand, these vibrations would result in real estate losses, particularly true for buildings used for activities which were sensitive to background vibrations (e.g. recording studio). In 2015, Connoly *et al* [7] documented a database of 56 commercial ground-borne noise and vibration reports with intention to assess the severity of such problem with sufficient details. The figure 1.1 illustrated the possibility of the predicted ground-borne vibrations caused by high-speed train which exceed the national/international allowance limits based on the reports from the database. The accounting for 44% exceedance in the corresponding section manifested the importance

of this railway assessment, and the ground vibration is a vital consideration for most projects.
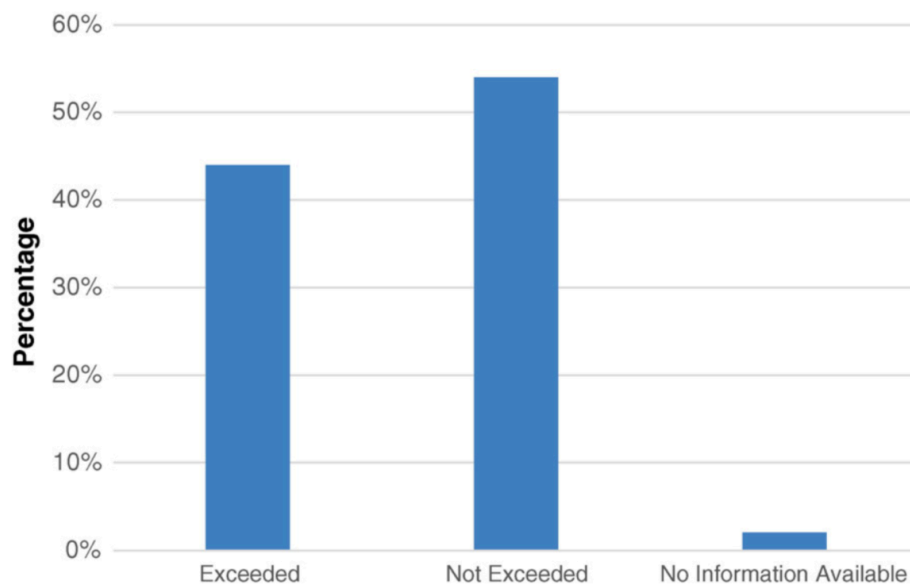
Figure 1.1 – The likelihood of ground-borne vibration threshold exceedance from the database

The evidence was clearly revealing that the ground-borne vibration caused by the passage of high-speed train was becoming a nuisance to many [8]. Hence, it may be of interest to find an approach to isolate the surroundings from the railway, or to mitigate the level of oscillations through the earth. In the context of this manuscript, the knowledge of the causality of vibrations was provided in the following literature review, along with the possible solutions to overcome the excessive devastations.

1.2 Literature review

1.2.1 Vibration generation

The generation of vibration is solely a consequence of the vehicle's forces passing from the wheels into the tracks and will propagate outwards [5, 9]. They arise from the weight of the train(quasi-static excitation), from changes in supportive stiffness(equally spaced sleepers) and irregularities in wheel/rail geometry(dynamic excitation) [10]. The quasi-static forces are independent of the train speed. They are dominant in track responses and near field, causing local deflection of the track under each wheel. In exceptional

cases, they can lead to the "bow wave" effect in the ground which only exists when the train's speed goes beyond the wave speed in the ground [11]. The formulation for the track's displacement due to the running train has been well-established [12,13].

On the contrary, dynamic excitation is time dependent and gives rise to the stiffness variation at the sleeper placement, or to the irregularities in the geometry between the interface of the wheels and tracks. However, this dynamic excitation from the geometric irregularities and railway track joints are becoming a less significant excitation mechanism, thanks to the improved track maintenance and to the widely used techniques of seamless welding in railways. Yet, the wave propagation away from the track is an inescapable concern.

1.2.2 Wave propagation

Given that the vibrations are being generated by the interaction between trains and tracks, parts of the energy are transmitted from the vibrating source to the all dimensions as the form of waves, while other parts of energy are dissipated as heat. Putting sound waves aside, these waves are commonly classified into either body waves or surface waves [13]. Body waves primarily move through the interior of the earth. Conversely, surface waves are typically generated when the vibration source is close to the structural surface, over which they travel, decaying exponentially with the depth.

The seismic waves consists of two different types: compressional waves (P-waves), which propagates in a longitudinal direction, and shear waves (S-waves), which propagates in a transverse direction. The P-waves commonly travel faster than other types of waves, then followed by the S-waves. Another type of waves is known as the Rayleigh waves, which include both longitudinal and transverse motions that decrease exponentially in amplitude as the distance increases from the surface [14,15]. They have the lowest travel speed among seismic waves and the speed is highly dependent upon the constitutive wave components (P and S waves).

Compressional, shear and Rayleigh waves are the most common seismic waves come across in the ground vibration scenarios, in spite of the possibilities to meet other types of waves such as Lamb's waves in layers and Stoneley waves at interface. In addition, a significant emphasis is put on the Rayleigh waves over all other types of waves in this project, the reason being that Rayleigh waves carry the nearly two thirds of the excitation energy during the transmission. Therefore, Rayleigh waves are most likely to have a negative influence in both railway tracks and nearby structures. In this contribution,

the main focus will be on eliminating the range of frequencies that cause the harmful disruptions.

1.2.3   Damaging frequency range

As it has been mentioned earlier in section 1.2.1, there is a large number of train components generating the excitation mechanism that covers the frequency spectrum from low to up to high, many of which can be seen in the figure 1.2. It can be found that the frequencies caused by the locomotive (blue charts) of train tend to be at a lower range and the excitation associated with the wheels, rails and tracks (red charts) tend to be at high frequencies. Noticing that the upper soil layer vibrates at the threshold of the lower limits of both ground-borne noise perception and human hearing. It is worth discovering that the upper limit of ground-borne vibration perception almost processes half of the vibration frequency range of the running train. Studies have found that ground vibrations from trains manifest themselves in two ways: in the low frequency range (between 1 and 80 Hz), the lineside buildings perceive the vibration as a mechanical vibration of the human body, whereas for high frequencies (between 16 and 250 Hz), the vibrations lead to structure-borne noise radiating inside the buildings due to the vibration of walls and floors [16–18]. According to several credential international standards and regulations, the damaging frequency caused by trains can be referred to the table 1.1.
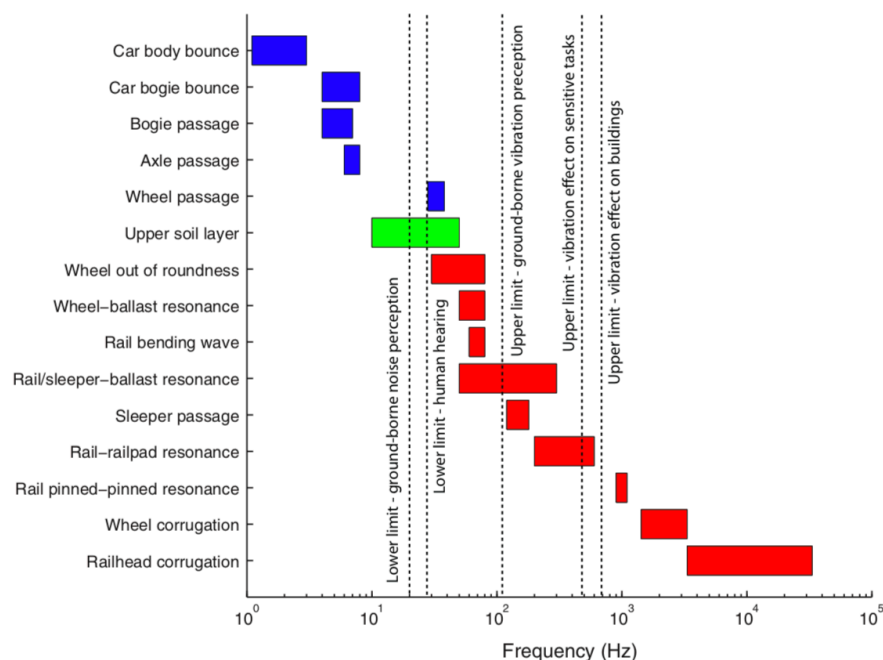
Figure 1.2 – Typical frequency range of excitation from a running train

Table 1.1 – Regulations that have defined the damaging frequency range

Organisation	Comments	Frequency	Refs
ISO 2631-1/2	human comfort and shock in buildings evaluation when exposed to whole-body vibration	0.5-80 Hz	[19, 20]
USDT[1]	assessing potential impacts on residential structures resulting from the high-speed trains	15-40 Hz	[21]
BS ISO 14837	frequency from train vibrations that are transmitted on soft soil	5-50 Hz	[22, 23]
DIN 4150-2/3	German standards which are used in Germany, Belgium and other European countries	NA	

The ground-borne vibration of low frequency caused a series of damage to human perception and gave rise to the noises inside the buildings, which will potentially have a chronic impact on the structural integrity and thus it is addressed in the international standards. ISO 2631 [19, 20] evaluated the vibrations in accordance with the root-mean-square (RMS) value of the acceleration in the three orthogonal directions. Furthermore, the later ISO 14837 [22, 23] developed dedicated standards on soil transmission. The summaries from the standards and international organisations disclosed that the damage frequency range were approximately between 10 and 80 Hz (see from table 1.1), most of which was transmitted through the ground. Hence, it is of important to understand the characteristics of the soil configurations and its influence on the wave propagation, especially to the interest of the damaging frequency range. Although many efforts have been put into the development of the train-track resonant, like conditions where, if possible, the natural frequencies of the track could have been estimated, their effects and interactions with the underlying soil are still undergoing a large number of researches [15].

1.2.4 Soil modelling

The ground plays an essential role in the consideration of ground-borne vibration as it acts as a medium that allows the wave to propagate and eventually reach the nearby structure. It is often treated as a series of parallel soil layers [17, 18]. The soil layer is

---

[1]USDT is the abbreviation of U. S. Department of Transportation (Federal Railroad Administration)

usually composed of a shallow surface layer overlying a stiffer one, where the induced vibration is primarily determinant for the commencing of a high vibration level above a threshold frequency (also know as the cut-on frequency) which relies on the layer thickness and on the travel speed of the wave within this upper shallow layer [24]. So far, a large amount of work has been undertaken into the soil Elastodynamics waveform modelling, with initial analysis accomplished by [25] and developed by the successors Wang and Achenbach [26] who delivered an analytical expression as to illustrate the wave propagation being that confined within a homogeneous half-space caused by a stationary point load. Nonetheless, the practice challenge of thoroughly understanding the soil behaviour when integrated with the track/train model still remains. The earlier analytical solution seemed, unfortunately, less adaptive than it was thought to be, regardless the numerous researches [27] that have been dedicated for building the analytical model thereafter. These challenges implied the limitations of using analytical approaches, meaning that there was a growing consensus on addressing the problem with numerical methods because they were more suitable for mimicking the responses of soil on the basis of aforementioned complexities [10].

The most common approaches of numerical methods were summarised in the table 1.2.

Table 1.2 – Summary of the numerical methods for ground modelling

Method	Comments	Refs
FDTD[2]	using centre differencing integration scheme to approximate seismic wave equations	[28]
FEM	using a weak form of the wave equation; applicable to high complex geometries	[29–31]
FE/BE	FEM coupled with BE; BE only requires mesh at boundary and incorporates the use of Green's function for wave formulation	[32, 33]

To begin with, the finite difference time domain (FDTD) applied strong formulation of the seismic wave equation to simulate the manner of wave propagation [9, 28]. It usually discretises the domain into components of velocity and stress respectively. It was found that by doing so, this method was more computationally efficient compare to other alternative numerical methods (e.g. [34, 35]), because the widely acceptance in velocity/stress mathematical model allowed to ease the workload by dividing it, if necessary,

---

[2]FDTD stands for the finite time domain method

into several computers if necessary. Additionally, PMLs (perfectly matched layers) have been effectively implemented to absorb the boundaries in order to prevent it from incoming boundary reflections. The advantages of FDTD have made it turn into a useful tool when investigating the railway problems [36, 37]. Although the strengths of FDTD are obvious, this method offered a considerable challenge in modelling complex geometries and free surfaces. Another weakness was that it required many assumptions to formulate the analytical expression and therefore it had a reduced performance in including the complex changes to geometry or to calculating the structural vibrations [10]. This drawback limited the use of FDTD in appraising the soil mitigation as a detailed soil model construction, where flexible interventions in parameters were essential in this scenario.

An alternative, or rather improved, approach to FDTD is the finite element method (FEM). Perhaps FEM is the most commonly used numerical technique, not only for the superior suitability in a variety of complexity, but also in the outstanding performance in returning solutions. The simulation process of FEM can be coupled with other graphical interfaces such as ABAQUS and ANSYS, and with a number of commercial software [38, 39]. Due to the advantages of modelling complex geometry, FEM can effectively exhibit the behaviour of rail track and other associated components. Despite of it, FEM does not enjoy the overwhelming superiority in terms of computational efficiency. Furthermore, as the size of the domain increases, the running time consequently become prohibitive, which makes it burdensome when coping with large offsets [9]. Given the weakness of time domain in FEM, an alternative approach is to reformulate the process and perform FEM analysis in frequency domain instead of time domain. Frequency domain FEM requires a solved eigenvalue for each frequency of interest in order to reduce the overall computational expense in time. However, the major disadvantage comes with the fact that the majority of time domain absorbing boundary conditions (ABC) are not applicable in the frequency domain. Hence, it is difficult to absorb unwanted reflections from the boundary.

In an attempt to simulate wave propagation in large domains, the FEM method can be overcome by coupling FEM with the boundary element method (BEM) [40]. The boundary element method significantly reduces the meshing requirements from the whole-body to merely boundaries; it formulate the wave propagation by using the Green's function, which is novelly suitable for large offsets and is in favour of use in the railway applications. FEM models the complex track configuration in near-field while BEM is utilised for far-field vibrations. The FE/BE method can be formulated in both time domain [41]

7

and frequency domain [42], but bias to the frequency domain in practice because of greater accommodative in manipulation.

By understanding the description of mathematical models for soil behaviour as a result of the vibrations that were induced by trains, a number of ground alleviation methods were developed afterwards.

1.2.5   Mitigation methods

As mentioned in section 1.2.4, the ground configuration is often regarded as having two layers, with a soft layer overlying the stiffer one. The results have found that the soft upper layer usually has a thickness of 2-6m and its corresponding cut-on frequency is between 10-30 Hz. In general, the ground-borne vibrations become magnified in the range of 10 to 40 Hz and this must be carefully taking into account when addressing the vibration extenuation methods [43].

In principle, there are a number of ways to reduce the vibrations induced by the passing trains. Moreover, the philosophy of the ground vibration attenuation is similar to that of the methods applied in diminishing mechanical noise. According to Lutz Auersch [44], the directions of mitigation methods can be classified into three major categories: the vibration source (train/track interfaces), transmission path (soil/ground) and the receiver (structures/humans). For instance, the changes to the vehicles of the train have been studied by [45], improving the tracks [46] as to achieve a better operation, and as to effectively prevent concrete constructions [47]. As a matter of fact, this thesis will emphasise on the approaches that have been implemented on the transmission path, which is of the major interest to the objectives.

Furthermore, since the soil ground is often treated as a continuum medium, one possible and obvious solution is to create such a discontinuity somewhere along the transmission path that would cut out transmission continuity along the route so that it mitigates the vibrations afterwards. This typical discontinuity can be achieved with an open trench, which is commonly used to reduce ground vibrations from machinery, and which is similar to the function of a noise barrier. The vibration waves were diffracted at the trench boundaries and only a small portion of the original waves passed through, thus the overall vibration was reduced. However, this ideal concept of open trench has a major limitation. Research [48] have discovered that the conceptual open trench becomes very unstable to hold the shape whilst maintaining the uniform attenuation function as it is meant to do. So, in practice, it requires reinforcement along the depth. Alterna-

tively, sloping sides can also assist in the service. On the contrary to an open trench, this open space can be filled with some other materials. Softer materials are usually recommended as they can efficaciously reduce the ground-borne vibrations by introducing different inclusions in ground compositions, but softer material should also satisfy other design factors such as the capability of balancing the earth pressure. Sometimes the soft materials will be over-compressed under the vibrating conditions so that the initial flexible materials may become stiffer, which would then increase the impedance and resulting in a loss in its isolation ability, even cause counterproductive effect [49]. Although it was argued that the use of filled trench is less effective compared to an open trench because of the former method which still allows for vibration transmissions as well as wave diffraction, both, open trench and filled trench, are still commonly employed in engineering applications as means of isolation [50], on account that the shielding performance is able to deploy without needing excessive expenses on finance and without difficulty to realise it.

Many scholars and engineers have yielded a large amount of numerical methods to formulate the trench models used for analysing the influence of different properties on the vibration mechanisms [8, 24, 44, 49]. Yang and Hung [51] constructed a 2D FE open trench model and acquired a surprising Poisson' ratio change in soil, leading to a conclusion of extension in trench depth which achieved effective performance in vibration attenuation. Adam and von Estroff [52] considered both, open trench and an in-filled trench with material of soil-bentonite, and formulated them into the frame of a coupled 2D FE/BE model. A 3D model was investigated by Anderson and Neilsen [8], who had taken into considerations other options of filled materials such as rubber chips.

On the other hand, there were only few experimental studies being carried out on fullscale site test. In addition, laboratory works have only just paid attentions to particular scenarios instead of substantially comprehensive investigations. It is worth mentioning that the trench model is usually integrated with the surrounding soil configuration, therefore the effect of soil characteristics such as homogeneity and layering are also being studied by [53]. The simulation was built under the condition of plane-stress in order to investigate formulations for the wave screening efficiency of vibration isolation within a confined frequency domain (refer to section 1.2.4). From the previous studies of numerical methods, it was consistently found that the implementation of trenches gave rise to effective performance once the trench's depth was approximately half of the Rayleigh wavelength, which is the dominant type of waves in ground-borne vibration. Nevertheless, trenches are sometimes limited in cases where the depth required

by the method influences the underground's infrastructure such as pipelines.

Subgrade stiffening is often considered as an alternative approach. In the perspective of reducing the settlements and track's displacements, the subgrade stiffening serves to improve the soil underneath the track, especially for intrinsic soft soil [54]. This technique was further explored to reduce the level of ground-borne vibrations by introducing a layer of stiffer materials beneath the rail tracks and by dampening out the transmitted vibrations at lower frequency range for all types of vehicles. Through the engagement of numerical models and together with the associated site experiments, it was found that the intervention positioned under the track was the most efficient lay-out. The problem was overcome by making alterations in conventional lay-outs, whereby subgrades took place next to the rail track. The figure 1.3 demonstrate some possible lay-outs from literatures.
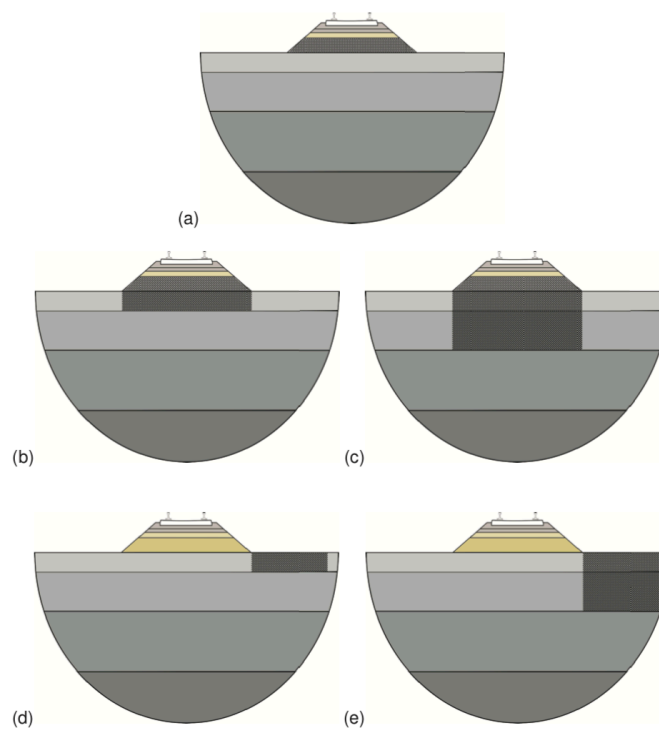
Figure 1.3 – Several possible subgrade stiffening lay-outs: (a)stiffening of the embarkment; (b)-(c)stiffening of the embarkment and the top layer; (d)-(e)soil stiffening next to the track

There are a number of soil improvement strategies which are successfully served to attenuate the level of vibrations in practice and in accordance with the subgrade stiffening

techniques. The following descriptions summarise some countermeasures and briefly state their principles.

- **Deep vibro compaction**
  The principle follows the reduction of pore granular contents in order to achieve a higher density combined soil configuration, thus an increased stiffness. The technique is suitable for densification of gravel and sand. But the densification is limited by the presence of slit and clay as they may have severe consequences. [55, 56]

- **Deep soil mixing**
  Deep soil mixing is a form of soil improvement involving mechanical mixing of soft and weak soils, usually being a combination of cement and lime in different proportions. This technique can be applied to a wide range of ground features such as cohesive deposits, soft clays and loose sand [55, 57]. Through the reinforcement of elements of compressibility and shear strength, the soil mixing technique drives the soil towards the state of reduction in subsidence, increment in shear and high bearing capacity of the composite soil mass. Hence, a significant filtration in the ground-borne vibrations that induced by high-speed trains. This counter-plan has been used in Sweden by Banverket. Moreover, it has also been used in the rail tracks between Rawang and Bidor in Malaysia for the passage of HST [57].

Apart from the contents mentioned afore, there existing other similar techniques that can be applied in ground treatments such as stone columns, grouting or vacuum consolidation. A holistic and systematic summary of these techniques can be referred to RIVAS [54]. Whilst it is true that the subgrade stiffening is a possible approach in many situations, it should be bore in mind that the financial cost of such deployment is considerably high and engineering difficulties during the practical construction are gigantic. Seeking to further optimise the techniques, with respect to the distinction of filling materials, their arrangement in geometry has reached a consensus among engineering study.

1.2.6 Stop band phenomena

Arousing from the techniques presented in the previous section 1.2.5, the intervention in the original soil configuration contributed in a significant impact on the wave propagation. The finding of such phenomena can be ascribed to the difference in the behaviour of heterogeneous materials from their counterpart homogeneous materials when both

of them are subject to dynamic loading conditions [58]. It was well understood that wave is one type of energy. As wave propagates through an elastic medium, the energy dissipates in the forms of heat and sound. As a results, the oscillatory displacement declines as the distance increases from the vibrating source. However, it was also found that waves propagating in the heterogeneous structure exhibit a wide variety of interesting dynamic effects, especially in periodic or random composites [59]. One of these striking phenomena is known as *stop-bands* (or *band-gaps*)- a frequency domain where little permittivity of wave propagation is allowed, regardless of transmission directions [60].

The stop band was originally found in the photonic crystals. Typically, as in marcostructure where these photonic crystals are arranged in a manner of periodic arrays of two materials which differ in certain properties, the light, as a form of electromagnetic waves, are prohibited for transmission in neither longitudinal nor transverse direction. Furthermore, it is noteworthy that there existing considerable similarities between the properties of periodic elastic composites and periodic dielectric. Hence, a tremendous research interest in the details of so-called phononic(acoustic) band gaps has led to the development of comprehensive theories of revealing the mechanisms inside the microscale [61]. There are two well-known theories for phononic stop bands, namely Bragg scattering theory and local resonance theory respectively.

According to Bragg's theory, the casualty of stop band is due to the loss of the possibility of elastic wave vibration modes [58]. However, this theory cannot properly explain the phenomena at a lower frequency (below 1KHz). In contrast to Bragg's scattering theory, Liu's local resonance theory presented that the existence of stop bands in elastic wave propagation is due to the interaction between the wave and the composite material. As a result, when the resonance happens to be out-of-phase to the incoming wave modes, there is not any exhibiting propagation phenomena thanks to the annihilation between the two waves [58, 62].

To gain a better insight into the characteristics of the stop bands when materials are subjected to imposed dynamic loading, also investigating the qualitative and quantitative behaviour of the transmission inside the passband, a number of studies have been undertaken experimentally and theoretically. Vasseur et al [63] have performed an experimental of a 2D solid composite made of squares and rectangulars in order to analyse the transmission of elastic waves in both air and water. In addition, inspired by Vasseur, Zhang et al [64] found that the combination of steel/epoxy presented two stop bands (100-200 kHz and 340-400 kHz) that strongly agreed with the results that numerical simulation predicted. Although experimental results have demonstrated valuable discover-

ies, due to the practical difficulties in manufacture of such composite in microstructure, of special interest, a great amount of investigations have undertaken in the numerical solution field for the sake of economy and time. Also, different methods have been proposed to study the frequency stop bands. For instance, the plane-wave expansion (PWE) method [60, 65], the Korringa-Kohn-Rostoker (KKR) method [66, 67], the multiple scattering (MS) method [68], and the finite difference time domain (FDTD) [69–71]. Among the listed methods, PWE, MS and FDTD are the most commonly used approaches. The methods mentioned above were hampered in this project by their complexity and time consuming, therefore, in this research, the gradient elasticity theory [72] was introduced as an alternative way to calculate the stop band in a more efficient but also in a more reliable approach. The detailed methodology will be given in the section 2.

Notwithstanding, the stop bands have occurred in periodic composites which were proved by literatures and some findings also demonstrated a curious phenomenon in which the randomness in materials also contributed to the effect on forbidding elastic vibration modes. Nakashima and his co-workers studied the influence of randomness on material's geometry in 2D scenarios, and found that the position change of inclusion caused a reduction in wave transmission as compare to the original periodic arrangement. However, the results were weakened by the inadequate experiment data and led to the research being less conclusive. In a parallel study, a striking conclusion was drawn by Liang and Patil [73]: not only did randomness create a noticeable difference in wave propagation, they were also capable of shifting a stop band into a passband, provided appropriate adjustment in randomness at some frequencies.

In this project, randomness on both material's mechanical and geometrical properties will be introduced in order to investigate the the associated influence on the elastic stop band. Of special interest is the prospect of accomplishing stop bands in the range of vital damaging frequencies that are produced by the passage of high-speed trains. Additionally, the degree of sensitivity to the stop band, cause by the addition of randomness, will be studied, from which the optimal selection of two-phase materials will be allocated.

1.3   Aim and scopes

The motivation of this project was inspired by the presence of *stop-band* or *band-gaps* in wave dispersion as a results of periodic heterogeneous materials. The purpose of this project is to propose the use of heterogeneous material combination as a possible solution to attenuate the vibrations induced by high-speed trains, with explicit indication to supply the knowledge of the corresponding mechanical and geometrical properties.

The main objectives to accomplish the aim of the project are presented below:

- To predict the analytical stop band frequency, from which the characteristics of the potential material combination can be identified;

- To construct one-dimensional laminated model and process systematic analysis on the mechanisms, whereby

    - analysing the effect of mechanical contrast ratio;
    - analysing the influence of geometrical features;
    - analysing the impact of the material's periodicity with regards to its mechanical and geometrical characteristics.

- To open up a tangential avenue for the future study through the synthesis of the literatures reviewed afore.

1.4   Outline of the thesis

This thesis is divided into 5 sections:

- *Section 1*   Introduction to the motivation of the research's projects and documented relevant background information, along with the scope and objectives.

- *Section 2*   The first stop band frequency within heterogeneous material was studied through the numerical method.

- *Section 3*   A one-dimensional laminated model was constructed to simulate the mechanisms of the mitigation measure in vibration. Graphical interpretationS were performed.

- *Section 4*   This section concludes the project.

- *Section 5*   Envisioning the future development in this project.

2 STOP BAND PREDICTION

In section 1.2.6, by balancing the weight of most commonly used numerical methods for calculating the stop bands, the gradient elasticity method was chosen to be in favour of adoption in the current project, the reason being a reduction in its complexity as well as less time consuming. The greatest advantage of the gradient elasticity theory is perhaps the formulation of the stop band which can be effectively predicted without explicit definition of material's properties whilst it is inclusive to all essential information of the corresponding microstructure [58].

2.1 Introduction to gradient elasticity theory

The conventional continuum solid mechanics is a mathematical study used for characterising deformation behaviour in materials at a wide range scales from nanometers to even earth size scales. The principle of continuum mechanics is that one can associate a particle of matter with each and every point of the region of the space possessed by an object, whilst credit the field quantities (e.g. density, velocity and so forth) to these particles [74]. In general, material deformations can be categorised in accordance with elasticity and plasticity [75]. The fundamental elasticity, Hooke's Law, has been widely used in engineering field ever since Robert Hooke discovered the linear proportionality relationship between the applied force F in an uniaxial tensile test of a solid bar and the change in axial length Δu through a spring constant k_s.

$$F = \Delta u \times k_s \qquad \text{Equation 2.1}$$

Then the equation 2.1 extended to relate the stress and strain for a given material.

$$\sigma = E \times \varepsilon \qquad \text{Equation 2.2}$$

where σ is stress in axial direction, E is Young's modulus of the material and ε is strain in axial direction. However, the equations so far is only indicated the relation in one-dimensional cases. For a continuum material, generalised Hooke's Law defines a more generic linear relation among all the components of stress and strain tensors, see equation 2.3

$$\sigma_{ij} = C_{ijkl} \times \varepsilon_{kl} \qquad \text{Equation 2.3}$$

where, in this expression, C_{ijkl} is a constitutive matrix and consists of components of the fourth-order stiffness tensor of material properties or *Elastic moduli*, whereas σ_{ij} and ε_{kl} are stress tensors and strain tensors respectively. The generalised Hooke's law (equation 2.3) can be used to address two-and three-dimensional continuum problems with increment in the size of constitutive matrix C as the dimension increases. Nevertheless, the classical elasticity theory is only valid for homogeneous materials. The overall physical behaviour of heterogeneous materials heavily relies on the size, shape, properties and spatial distribution of the micro-structural constituents. For heterogeneous materials, the results given by the classical elasticity gradient theory violate the physics in a microscopic level. In the prospect of achieving a complete understanding of both statics and dynamics in heterogenous material, the gradient theory is further developed by enriching the field equations with appropriate higher-order spatial gradients of state variables [58]. Meanwhile, homogenisation techniques also taking place in this process of transforming the heterogeneous to homogeneous in order to create an equivalent continuum mass [76].

A number of extensive gradient theories have suggested the additions in gradient strain. In this section, Aifantis' [77] theory and Eringen's [78] theory will be treated in chronological order, together with the unified manner initiated by Metrikine and Askes for the response of a discrete material model [79].

2.1.1 Eringe's theory

Eringe's work emphasised the use of an integral-type of nonlocality, in which volume averages of state variables were calculated. The formulation of this gradient theory was acquired from the dynamic point-view. The nonlocal stress tensor is given in equation 2.4

$$\sigma_{ij}^g(x) = \int_\Omega \alpha(s) \cdot \sigma_{ij}^c \cdot (x+s) \cdot d\Omega \qquad \textbf{Equation 2.4}$$

where σ_{ij}^g is the stress tensor by the gradient theory, $\alpha(s)$ is a nonlocal weight function which is a non-negative value and normally decreases as s increases. Moreover, σ_{ij}^c is the local stress tensor which relates to the gradient displacement, that is $\sigma_{ij}^c = C_{ijkl}u_{k,l}$. In 1983, Eeingen further explored the above formula and replaced spatial integrals by differential operators. It is important to bear in mind that the error caused by this mathematical approximation strongly depended on the definition of the weight function $\alpha(s)$.

The final result is presented as a partial differential form:

$$\sigma^g_{ij} - l^2 \sigma^g_{ij,kk} = \sigma^c_{ij} = C_{ijkl} u_{k,l}$$ **Equation 2.5**

where l is an internal length-scale parameter, the magnitude of which follows from the definition of nonlocal weight function $\alpha(s)$. Also, σ^g_{ij} and σ^c_{ij} represents the gradient stress tensors and the classical stress tensors respectively. The equation of motion is expressed as

$$\sigma^g_{ij,j} + b_i = \rho \ddot{u}_i$$ **Equation 2.6**

where ρ is the mass density.

The overall partial differential equation predicted by Eringe's gradient theory can be written as

$$C_{ijkl} u_{k,jl} + b_i = \rho(\ddot{u}_i - l^2 \ddot{u}_{i,mm})$$ **Equation 2.7**

2.1.2 Aifantis' theory

To get insight into the linear elastic constitutive relations based on the static point of view, Aifantis and his co-workers extended the original Laplacian strain energy density with an extra term, and the constitutive relation is then adapted to

$$\sigma_{ij} = C_{ijkl}(\varepsilon_{kl} - l^2 \varepsilon_{kl,mm})$$ **Equation 2.8**

where l is again a length-scale parameter, stress tensors σ_{ij} and stiffness tensor C_{ijkl} have the same meaning as in equation 2.7 and the strain remains the same as in classical elasticity, see equation 2.9

$$\varepsilon_{kl} = \frac{1}{2}\left(\frac{\partial u_k}{\partial x_l} + \frac{\partial u_l}{\partial x_k}\right)$$ **Equation 2.9**

where u_l and u_k are displacement components.

As one may notice, there is a clear similarity between equation 2.3 and equation 2.8, but the major change is that equation 2.8 contains higher-order spatial gradients of strain in comparison with equation 2.3. Besides, an additional length scale parameter l defined by the weight function α correlating the microstructure of the material.

The associated equilibrium equation is written in the same way as the classical theory:

$$\sigma_{ij} + b_i = 0 \qquad \textbf{Equation 2.10}$$

where b_i is known as the body force component. Substituting equation 2.8 into equation 2.10, the overall partial differential equation is obtained:

$$C_{ijkl}(\varepsilon_{kl} - l^2\varepsilon_{kl,mm}) + b_i = 0 \qquad \textbf{Equation 2.11}$$

2.1.3 Dynamically consistent gradient theory

The main motivation of using gradient elasticity in statics is to prevent from singularities in the elastic field, whereas the reason of applying the gradient theory in dynamic is to describe the wave dispersion. In order to achieve dynamic consistency, it is often important to compromise a combination of gradients which are simultaneously applicable to both statics as well as dynamics. The simplest version of a dynamically consistent model is given by the equation 2.12,

$$C_{ijkl}(u_{k,jl} - l_{stat}^2 u_{k,jlmm}) + b_i = \rho(\ddot{u}_i - l_{dyn}^2 \ddot{u}_{i,mm}) \qquad \textbf{Equation 2.12}$$

where l_{stat} and l_{dyn} are relevant length scales in static and dynamics, which can be related to the size of Representative Volume Element, see section 2.1.4.

The unification of the theories of Eringen and Aifantis is possible in a dynamic point of view []. A generic constitutive relation reads:

$$\left(1 - l_{dyn}^2 \frac{\partial^2}{\partial x_m^2}\right)\sigma_{ij} = C_{ijkl}\left(1 - l_{stat}^2 \frac{\partial^2}{\partial x_m^2}\right)\varepsilon_{kl} \qquad \textbf{Equation 2.13}$$

For the dynamic case, by combining equation 2.13 and the usual equation of motion $\sigma_{ij,j} + b_i = \rho\ddot{u}_i$, with assumption of vanishing of the second derivatives of body forces, the equation yields to

$$C_{ijkl}\left(1 - l_{stat}^2 \frac{\partial^2}{\partial x_m^2}\right)\varepsilon_{kl,j} + b_i = \rho(\ddot{u}_i - l_{stat}^2 \ddot{u}_{i,mm}) \qquad \textbf{Equation 2.14}$$

Hence, equation 2.14 accomplished the unification of the gradient theory of Eringen and Aifantis.

2.1.4   Relation with the size of representative volume elements

An effective approach to portrait the manner of heterogeneous materials is by homogenising (mentioned in section 2.1) the response of a Representative Volume Element (RVE) [80]. PVE quantifies the smallest size over which measurements can be taken to yield, a value of representative of whole. For periodic materials, RVE is the length of unit periodic cells. The primary motivation for using RVE is to effectively correlate L_{RVE}, a parameter with unit cell length, with length scale parameters of gradient theories, in which two different length scales are proposed: the length scale in statics, l_{stat}, and the length scale in dynamics, l_{dyn}. This scale transition requires an addition of higher-order gradients, resulting in so-called *second-order homogenisation schemes* [76]. Gitman and his co-workers [81] have derived the relationship between the static scale length, l_{stat} and L_{stat}, see equation 2.15 below:

$$l_{stat}^2 = \frac{1}{12} \times L_{stat}^2 \qquad \textbf{Equation 2.15}$$

Also, if this transition approach is extensively applied to dynamics, the strain gradients and acceleration gradients in equation 2.7 will relate to the static RVE size and the dynamic RVE size respectively. A similar relationship was identified to be

$$l_{dyn}^2 = \frac{1}{12} \times L_{dyn}^2 \qquad \textbf{Equation 2.16}$$

The comprehensive analysis of quantification of RVE for static scenario can be referred to [81]. After the homogenisation process, the extended set of equations of motion was derived to be

$$\rho u_{i,tt} - \frac{1}{12}L_{dyn}^2 \cdot \rho u_{l,mmtt} = C_{ijkl}u_{k,jl} - \frac{1}{12}L_{stat}^2 \cdot C_{ijkl}u_{k,jlmm} \qquad \textbf{Equation 2.17}$$

2.2   Homogenisation of a periodic laminate

From the study of wave dispersion through periodic laminated composites, Fish and his co-workers [82] managed to develop dynamic mechanism by the gradient elasticity theory with stable inertia gradients. It was also found that the internal length scale l can be related to the constituents' volume fraction, by which the fraction indicates the contrast in material properties within a unit cell length. In the demonstration of the figure 2.4, the laminate is comprised of two-phase materials, denoting 1 and 2 respectively. Whilst the total length of a periodic unit cell is denoted by l. The volume fractions are α for material 1 and $(1 - \alpha)$ for material 2.
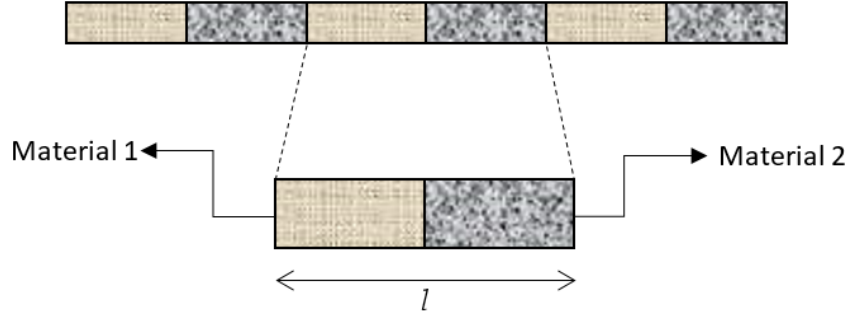
Figure 2.4 – The periodic laminated cell of length l comprising two different materials.

The equation of motion for homogeneous materials proposed by Fish and Chen is written as

$$\rho u_{,tt} = E u_{,tt}$$

Equation 2.18

where ρ is the overall effective density and E is the overall effective Young's modulus. The following equations are provided for calculation of effective density and for Young's modulus:

$$\rho = \alpha \rho_1 + (1 - \alpha) \rho_2$$

Equation 2.19

$$E = \frac{E_1 \times E_2}{(1 - \alpha) E_1 + \alpha E_2}$$

Equation 2.20

Now, with the next higher-order term included, the gradient theory applied in this calculation was modified from equation 2.18, as shown in figure 2.4, and can be expressed as equation 2.21:

$$\rho u_{,tt} = E u_{,tt} + \gamma l^2 E u_{,xxxx}$$

Equation 2.21

where l is the unit cell length of the periodic laminate, see in figure 2.4. The dimensionless coefficient parameter γ captures the impedance contrast of the two materials and is given through

$$\gamma = \left[\frac{\alpha(1 - \alpha)(E_1 \rho_1 - E_2 \rho_2)}{\rho((1 - \alpha) E_1 + \alpha E_2)} \right]^2$$

Equation 2.22

By substituting equation 2.21 into the harmonic solutions obtained previously, the wave dispersion is now written as below

$$-\rho\omega^2 A e^{i(kx-\omega t)} - \gamma\rho l^2\omega^2 k^2 A e^{i(kx-\omega t)} = -E k^2 A e^{i(kx-\omega t)} \qquad \textbf{Equation 2.23}$$

From which the frequency is deduced as

$$\omega^2 = \frac{E k^2}{\rho(1 + \gamma k^2 l^2)} \qquad \textbf{Equation 2.24}$$

By taking k to infinite, the first stop band frequency can be derived as

$$\omega = \lim_{k \to \infty} \sqrt{\frac{\bar{E} k^2}{\bar{\rho}(1 + \gamma k^2 l^2)}} \approx \sqrt{\frac{\bar{E}}{\bar{\rho}\gamma l^2}} \qquad \textbf{Equation 2.25}$$

2.3 Influential factors of the first stop band in periodic laminated materials

As it can be seen from the equation 2.25, the first stop band frequency which was predicted by using the gradient elasticity theory has a strong correlation with four parameters involved inside the equation, namely the overall effective Young's modulus E, the overall effective density ρ, dimensionless coefficient γ, and the length of unit laminate l.

Essentially, the first stop band formula can serve to identify the material's properties by knowing the value of the first stop band frequency. Alternatively, it can be used the other way round, as in giving the properties of two materials and work out the possible first stop band frequency value. The latter acts in a more active way than the former one. In addition, if two materials were acknowledged, the first stop band frequency will almost be derived as a certain fixed value. However, for cases of identifying the possible combination of two materials that will result in a desired stop band frequency, the solution simply reaches the field of a wide range of possibilities with less boundaries.

Reflecting on the purpose of this project, a reliable combination of heterogeneous material is of numerous interests. Considering the practical implementation, both of the materials here need to satisfy the basis of engineering constructions. Therefore, in order to reduce the range of possible combinations, the primary material was decided to be concrete, the information being given in the table 2.3.

Table 2.3 – The mechanical properties of concrete, resource from [3]

	E (GPa)	ρ (kg/m^3)	Tensile strength (MPa)	Poisson's ratio
Concrete	14-41	2240-2400	2-5	0.20-0.21

In the previous section 1.2.3, the damaging frequency range produced by the passage of high-speed trains was discovered to be mostly between 1-80 Hz [19–23], see in table 1.1. Therefore, the first stop band frequency determined by the gradient theory must,in this case, lay within this range. Furthermore, to accomplish a theoretical efficiency over 50%, the predicted stop band frequency was assumed to be no greater than 40 Hz, which is the average value of the fatal frequency range.

2.3.1 Modified equations

In this section, a systematic approach along with graphical interpretations will be served to elucidate the degree of impact of each factors within the equation 2.25 and on the variation of the first band gap frequency ω. To overcome the difficulties of having two separate properties for different materials, β was introduced as a relative ratio of the material's properties. For instance, β_E stands for the ratio of Young's modulus between material 1 and material 2 ($\beta_E = E_2/E_1$). Similar notations in density ratio, $\beta_\rho = \rho_2/\rho_1$. Hence, by replacing the properties of material 2 from the equations in section 2.2, a new set of modified equations were obtained.

- Overall effective density

$$\bar{\rho} = \alpha\rho_1 + (1 - \alpha)\rho_2 = \alpha\rho_1 + (1 - \alpha)\rho_1\beta_\rho \qquad \textbf{Equation 2.26}$$

- Overall effective Young's modulus

$$\bar{E} = \frac{E_1 \times E_2}{(1 - \alpha)E_1 + \alpha E_2} = \frac{E_1 \times E_1\beta_E}{(1 - \alpha)E_1 + \alpha E_1\beta_E} \qquad \textbf{Equation 2.27}$$

- Coefficient parameter γ

$$\gamma = \left[\frac{\alpha(1 - \alpha)(E_1\rho_1 - E_2\rho_2)}{\bar{\rho}((1 - \alpha)E_1 + \alpha E_2)}\right]^2$$

$$= \left[\frac{\alpha(1-\alpha)(E_1\rho_1 - E_1\rho_1\beta_\rho)}{\bar{\rho}((1-\alpha)E_1 + \alpha E_1\beta_E)} \right]^2$$

$$= \left\{ \frac{\alpha(1-\alpha)(E_1\rho_1 - E_1\rho_1\beta_\rho)}{[\alpha\rho_1 + (1-\alpha)\rho_1\beta_\rho]((1-\alpha)E_1 + \alpha E_1\beta_E)} \right\}^2 \qquad \textbf{Equation 2.28}$$

- The first stop band frequency

$$\omega = \lim_{k\to\infty} \sqrt{\frac{Ek^2}{\rho(1+\gamma k^2 l^2)}} \approx \sqrt{\frac{E}{\rho\gamma l^2}}$$

$$= \sqrt{\frac{\frac{E_1 \times E_1\beta_E}{(1-\alpha)E_1 + \alpha E_1\beta_E}}{[\alpha\rho_1 + (1-\alpha)\rho_1\beta_\rho]\gamma l^2}}$$

$$\omega = \sqrt{\frac{\frac{E_1 \times E_1\beta_E}{(1-\alpha)E_1 + \alpha E_1\beta_E}}{(\alpha\rho_1 + (1-\alpha)\rho_1\beta_\rho)\left\{ \frac{\alpha(1-\alpha)(E_1\rho_1 - E_1\rho_1\beta_\rho)}{[\alpha\rho_1 + (1-\alpha)\rho_1\beta_\rho]((1-\alpha)E_1 + \alpha E_1\beta_E)} \right\}^2 l^2}}$$

$$\textbf{Equation 2.29}$$

2.4   Material identification

In the final format of equation 2.29, the first band gap frequency ω is a function of primary material's properties(E_1 and ρ_1), laminate volume fraction(α) as well as the property contrast ratios(β_E and β_ρ). To simplify the expression, it can be written as the following equation:

$$\omega = f(E_1, \rho_1, \beta_E, \beta_\rho, \alpha, l) \qquad \textbf{Equation 2.30}$$

However, the only fixed known values are $E1$ and ρ_1, which are the properties of general concrete seen in table 1. Whilst the rest of the parameters will be chosen to vary in a certain range with linear manners. As there was a wide concern with the availability of the materials in the chart, the variation of the relative contrast for two materials, in which one happened to be concrete, is usually within a factor of 1000. In addition, the volume fraction for one periodic laminated cell is always between 0 and 1. The decision on the length of laminated cells will be discussed separately in the section 2.4.5. In the

interest of systematic demonstration, the range of those parameters are provided in the table below.

Table 2.4 – The range of variation of the essential parameters for calculating the stop band frequency

$E_1(GPa)$	β_ρ	β_E	$l(mm)$	α
23.3	0.01	0.00001-0.001	1500-3500	0.1-1

In the MATLAB analysis, both β_E and β_ρ were considered as being sets of column vectors with size of 10, meaning that the linearly increment value was 0.001. Similarly, the linear interval was taken to be 0.1 for the volume fraction α, with 10 additions covers from value 0.1 to 1. To gain a better insight into the individual effect of these state variables on the alteration of the stop band frequency, graphical interpretation was introduced in the view of providing qualitative and quantitative visualisations.

2.4.1 Overall effective Young's modulus

The overall effective Young's modulus variation with the Young's modulus contrast ratio β_E as well as the volume fraction α is demonstrated in the following figure 2.5.
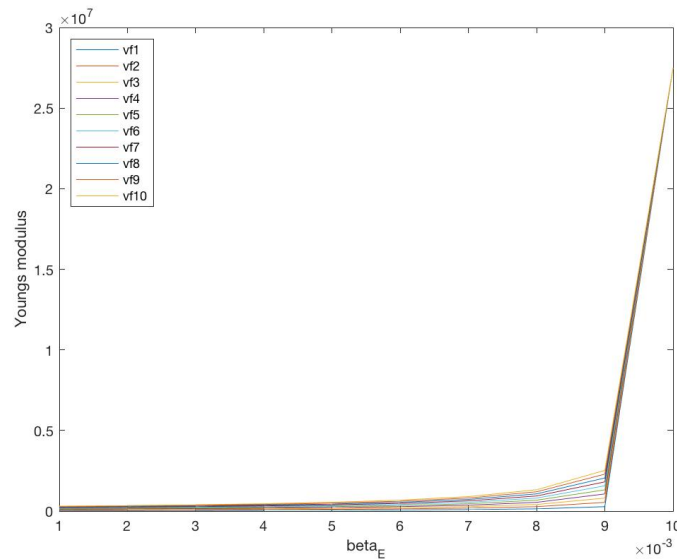
Figure 2.5 – The overall Young's modulus E varies as β_E increases linearly from 0.001 to 0.01; the legends stands for the variation for different volume fractions.

As it can be seen from figure 2.5, the general tendency showed a steady increase in the overall effective young's modulus from β_E=0.001 to β_E=0.009. However, the overall effective E suddenly sharped up right after β_E=0.009 and reached 27.5 MPa, where concrete property became fully dominant. It was noteworthy that the volume fraction α increased gradually from 0.1 to 1, as shown in the legend in the figure vf_1 to vf_{10}, resulting in small elevation in the value of the effective Young's modulus. Although a significant difference was noticed after β_E=0.006, this measured effect of volume fraction on the Young's modulus diminished at β_E=0.009 and all ten different lines of volume fraction squeezed up to almost a single line and kept growing with a steep gradient. A zoomed-in version can be seen in figure 2.6. Despite the fact that the effective Young's modulus was steadily increasing in the first nine property contrasts, the value of E was always confined between 0 and 3MPa. Additionally, a higher volume fraction (close to 1) came at a higher rate of growth in overall effective Young's modulus. For instance, infigure 2.6, vf_1 and vf_{10} are in both sub-figures.
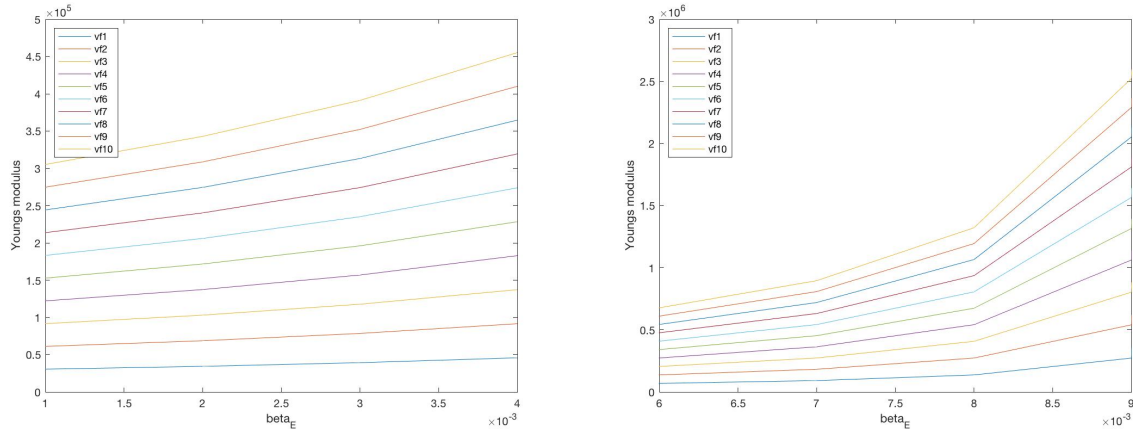
Figure 2.6 – A zoomed-in version of Young's modulus E against β_E; (left)axis between 0.001 and 0.004, (right)axis taken from 0.006-0.009

2.4.2 Overall effective density

In contrary to what dramatic and rather sudden impact that the effective Young's modulus demonstrated, the following figure 2.7 seemed to present a simple linear correlation between the effective density of two periodic materials and their density contrast ratio β_ρ. This linear correlation was also applied to every chosen volume fraction.
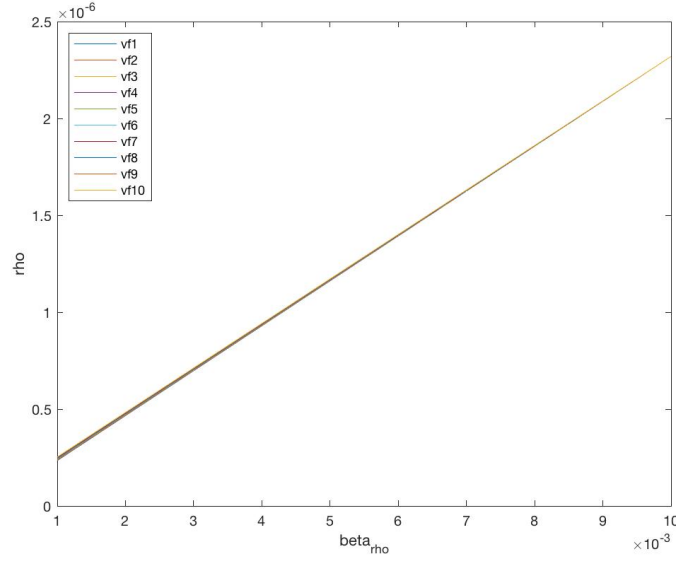
Figure 2.7 – The overall effective density ρ varies as β_ρ increases linearly from 0.001 to 0.01; legends stands for the variation for different volume fraction.

It can be seen from the obtained results given in figure 2.7 that the volume fraction of the laminated cell played an insignificant role on the overall effective density value. The top sub-figure from figure 2.8 showed a zoomed-in square taken between β_ρ=0.001 and β_ρ=0.002. The relative difference between each volume fraction was pretty minor in comparison with the impact on the density contrast.
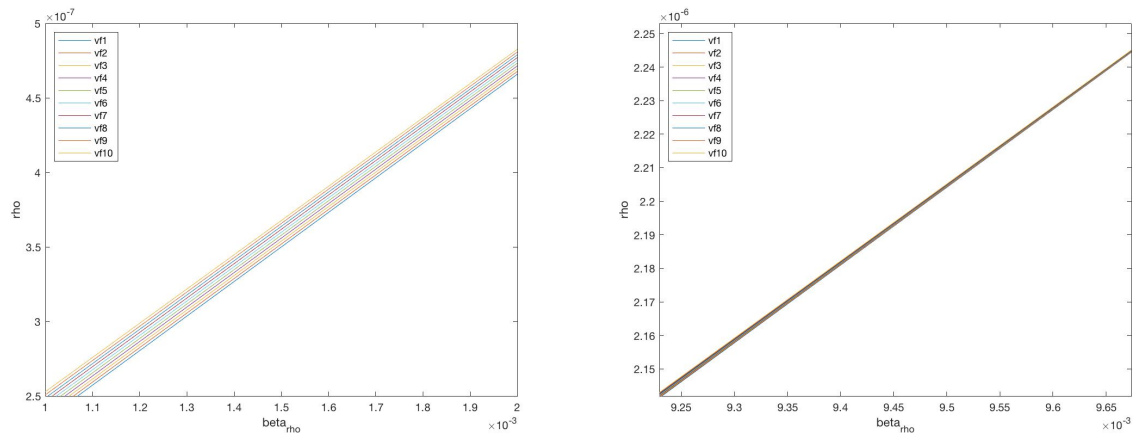
Figure 2.8 – A zoomed-in version of the effective density ρ against β_ρ; (left)axis between 0.001 and 0.002, (right)axis taken from 0.009-0.0097

Furthermore, as the density contrast became less influential (approaching 1), the den-

26

sity of concrete dominated the effective density and the effect on the volume fraction resulted in little changes in ρ, in spite of a much smaller β_ρ interval in the bottom sub-figure but still showing a more compact feature in the graph.

2.4.3 Coefficient parameter γ

The coefficient parameter γ is an essential dimensionless value which effectively relates to the impedance as vibration waves penetrate through the boundary of different materials. As it can be seen from the figure 2.9, the figure was presented in three-dimensional space as γ was affected by three different state variables. β_E and α accounted for the major variables, taken x-axis and y-axis. The third variable, β_ρ was set to be the master variable, by which the sets of β_E and α were assigned to each value of density contrast β_ρ and plotted into the same figure, resulting in a stack pattern as shown in figure 2.9.
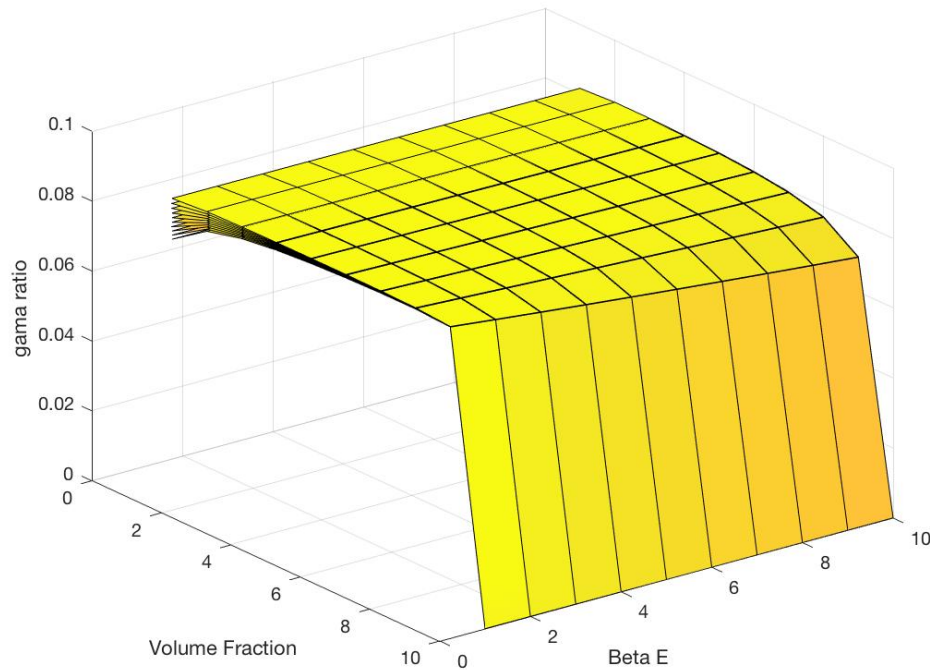
Figure 2.9 – The effects of both β_E and the volume fraction on the dimensionless coefficient γ for different value of β_ρ.

The majority of the values of γ were greater than 0.06 but less than 0.08 in which primary material was set to be general concrete. However, as the volume fraction α was approximated to 1, the γ value, all of the sudden, dropped down to 0. This is because of α equals

to 1, meaning that the primary material took over all the volume space and there was no difference in mechanical properties between two periodic materials. In other words, the original heterogenous system was developed into a fully homogeneous system and then produced no impedance at the interface between the boundaries. Consequently, the material will lose the ability to create a stop band frequency, as band-gap is only valid for heterogenous material. By and large, the effective γ is meaningful only if the volume fraction α is nowhere near 1.

The contrast ratio of Young's modulus generated indistinguishable results in γ values regardless the changes in β_E, except for α=0.8 and α=0.9, in which γ showed a slightly decrease as β_E rose from 0.001 to 0.01. The effects on γ due to the variation of β_E, apart from the ones just mentioned, were negligible. It is also worth mentioning that, as it was stated earlier, the third state variable was the contrast of density β_ρ. The staked pattern illustrated the impact of this third variable as a result of adding every single β_ρ to one figure.
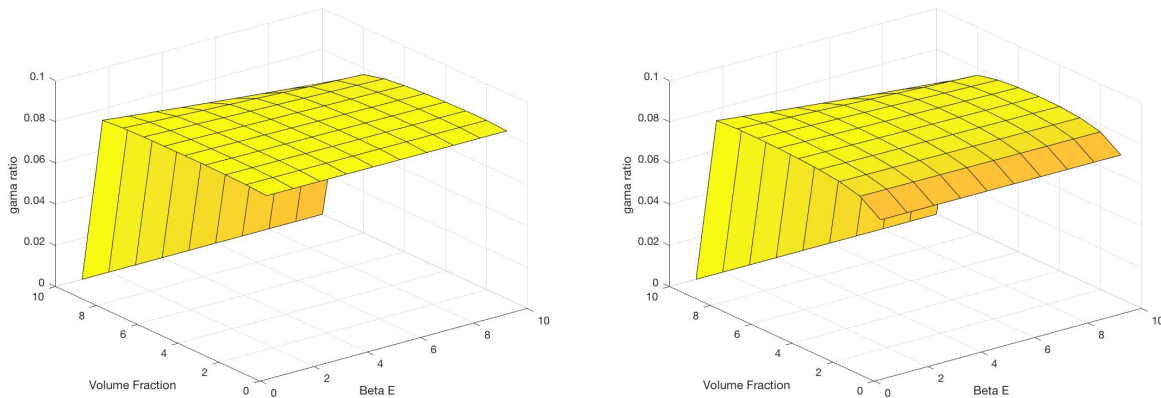
Figure 2.10 – The patterns of γ for the start and end values of β_ρ provided with full sets of β_E and α; top-figure for β_ρ=0.001; bottom-figure for β_ρ=0.01.

The following sub-figures (see figure 2.10) showed the two individual patterns of the start and end of the values of β_ρ. The contrast in density made a noticeable contribution in the γ particularly between $\alpha = 0.1$ and $\alpha = 0.3$, declining γ to below 0.08 but higher than 0.07. The most significant reduction was at $\alpha = 0.1$. The reduction converged to a steady level as α moved towards a bigger value. This is a common tendency for all other values of β_ρ. On the other hand, there presenting a very minimal relationship between β_ρ and β_E. The fact showed that the variations along the β_E-axis were all at horizontal lines no matter how much the volume fraction changed, with an exception for $\alpha = 1$, where the

whole system turned into a homogeneous scenario. To sum up, the geometrical feature and volume fraction, seemed to have had contributed the most impact on the fluctuation of the γ ratio. The mechanical contrast β_E and the density contrast β_ρ had substantial effects in vicinity of the extreme values of volume fraction α. That is to say, for higher volume fraction (α close to 1), the variation of β_E caused remarkable changes in γ; for lower volume fraction (α close to 0), differing in β_ρ resulted in a significant difference in γ. Nonetheless, it can be referred to figure 2.9 that, the higher density contrast(β_ρ towards 0), the greater γ ratio in general. And vice versa.

2.4.4 Stop-band frequency

Finally, the stop band frequency is a function of all five parameters indicated in equation 2.29. Taking into consideration of the reasonable range for the stated parameters, the following figure 2.11 illustrated the final version of how the first stop band frequency changes as those parameters differ within their corresponding ranges.
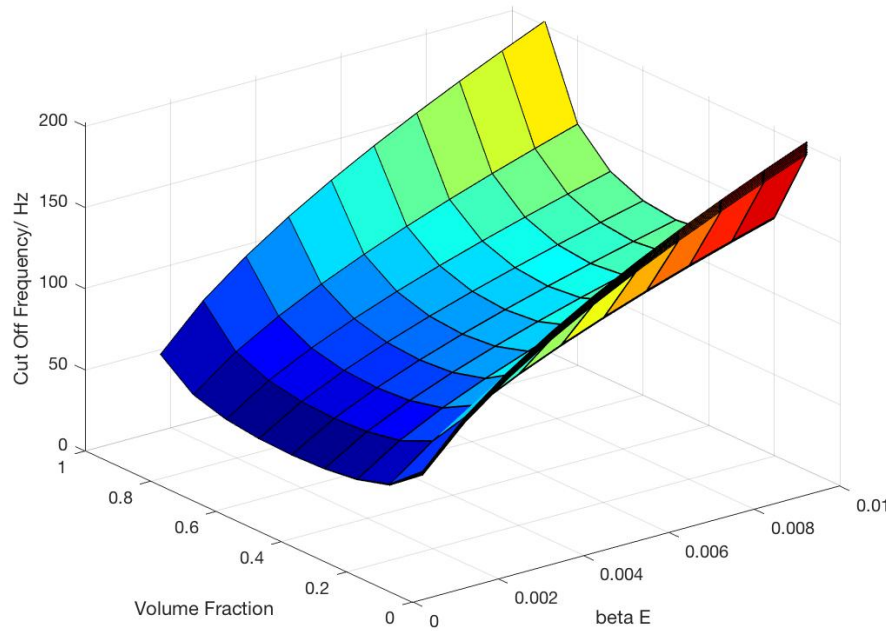
Figure 2.11 – The pattern of the influence on the first stop band frequency due to α, β_E and β_ρ.

It is important to bear in mind that, since the stop band frequency involved more than three state variables, it was challenging to present the influence of the frequency value

on each individual variable all in the same figure. In this case, figure 2.11 merely exhibited volume fraction α, mechanical contrast β_E and β_ρ due to the fact that they appeared most frequently in the modified stop band frequency equation 2.29, whereas, the length of the laminated cell l was testified later.

Similar to what was presented in figure 2.9, volume fraction α and β_E took over the variable dimensions: x-axis and y-axis. For each value of β_ρ, the complete sets of α and β_E formed a curvature-shaped pattern. By introducing the whole range of β_ρ, the curvature-shaped pattern added up and overlapped the other one demonstrated in figure 2.11.

It was obvious to see that β_E produced a decline tendency in the cut-off frequency when the mechanical contrast became large, namely β_E being close to 0.001. The impact of density contrast β_ρ remained insignificant. As a matter of fact, β_ρ only made minimal alteration in the cut-off frequency at lower values of the volume fraction α. As α was greater than 0.5, it was hardly to recognise any difference and all the patterns completely stacked together as one.
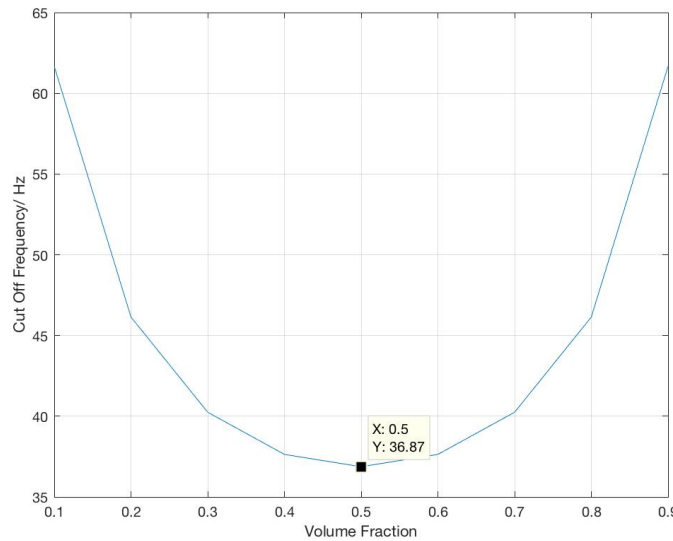
Figure 2.12 – The relationship between the first bang-gap frequency and the volume fraction, provided that $\beta_E=\beta_\rho$=0.001 and l=3000.

Volume fractions made a surprising contribution in the cut-off frequency. They displayed quadratic curves for each value of β_E. The local minimum point laid on α=0.5 for all cases. As it can be seen in figure 2.12, this curve was captured from figure 2.11 where the lowest cut-off frequency was located at β_E=0.001 and β_ρ=0.001. Therefore, it was right to say that the lowest cut-off frequency occurred at the highest contrasts of both mechanical property and density property and of equal size volume fractions

respectively. In addition, one may have noticed that there were only 9 points on x-axis in figure 2.12, namely 0.1 to 0.9. This is because, as mentioned earlier, the cut-off frequency could only be determined when α was not equal to 1 due to homogenisation effect resulting in missing of cut-off frequencies.

2.4.5   Length of laminated cell l

It was found that the length of laminated cells played an crucial role in determining the cut-off frequency. Since the contrast of density β_ρ had little effect on the cut-off frequency, in the investigation of cell length, it was decided to use β_ρ=0.001 as a fixed value of density contrast instead of the full range. By doing so, the cut-off frequency became a function of three variables, see equation 2.31.

$$\omega = f(\beta_E, \alpha, l)$$ **Equation 2.31**

The range of cell length was taken from 1500 to 3500, with 10 intervals and units in millimetres. The figure visualisation is presented in figure 2.13.
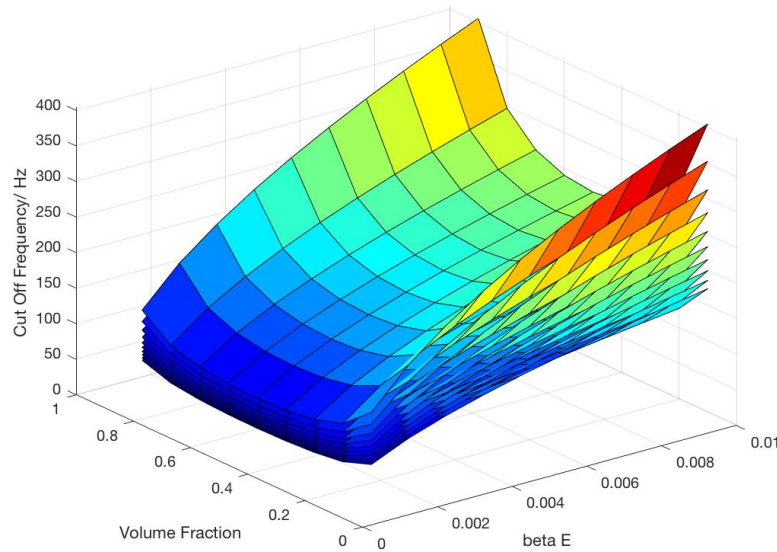
Figure 2.13 – The pattern of the influence on the first stop band frequency due to α, β_E and l.

Similar to what was presented in figure 2.11, in order to analyse the impact due to cell length l, each curvature-shaped pattern was formed at a value of l associated with com-

plete sets of β_E and α. By just looking at the lowest cut-off frequencies for each curvature pattern, the value of the cut-off frequency against the increasing length of the unit cell l was plotted in the figure 2.14.
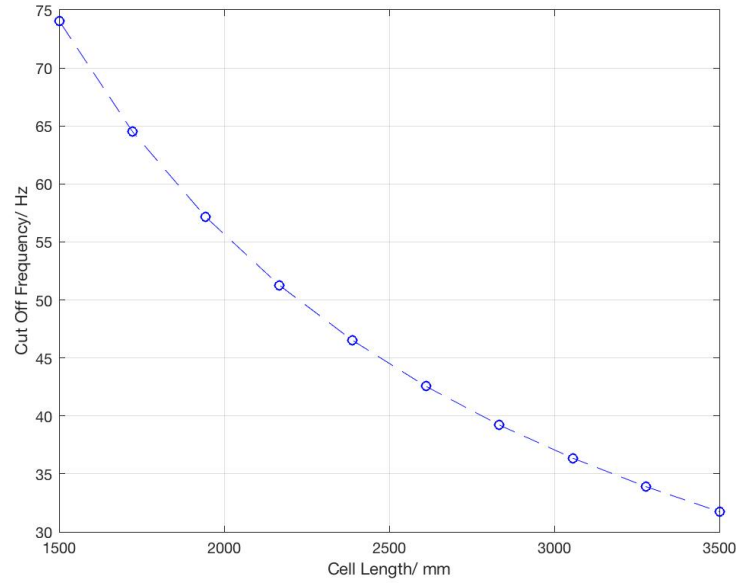
Figure 2.14 – The cut-off frequency changes with the laminated cell length l; the frequencies were captured at β_E=0.001 and β_ρ=0.001, along with α=0.5.

There was a clear exponential decay in the relationship between the cut-off frequency and the length of the laminated cell. Recalling the objectives of this paper, referring to both section 1.2.3 and section 2.3, the cut-off frequency was expected to appear as low as possible while considering the practical limitations. Therefore, 40 Hz (or below) was believed to be acceptable to use. As a consequence, the cell length was decided to be l=3000 mm, whose corresponding cut-off frequency was 36.87 Hz.

2.5 Results and discussion of material selection

As it was presented in figure 2.15, the chart has listed a number of materials for light and stiff components. The moduli of engineering materials span a range of 10^7; the densities span a range of 3000. By setting *concrete* as a reference material, whose $E_{concrete}$= 23.3 GPa, $\rho_{concrete}$=2.32 Mg/m^3, taking contrasts in β_E=0.001 and β_ρ=0.001 respectively, no solution, unfortunately, was yielded in accordance with these criteria because of the excessive density contrast. Note that, for the primary material to be concrete, the avail-

able density contrast was, according to figure 2.15, within the factor of approximately 100. Hence, the largest density contrast β_ρ, in this case, was 0.01.
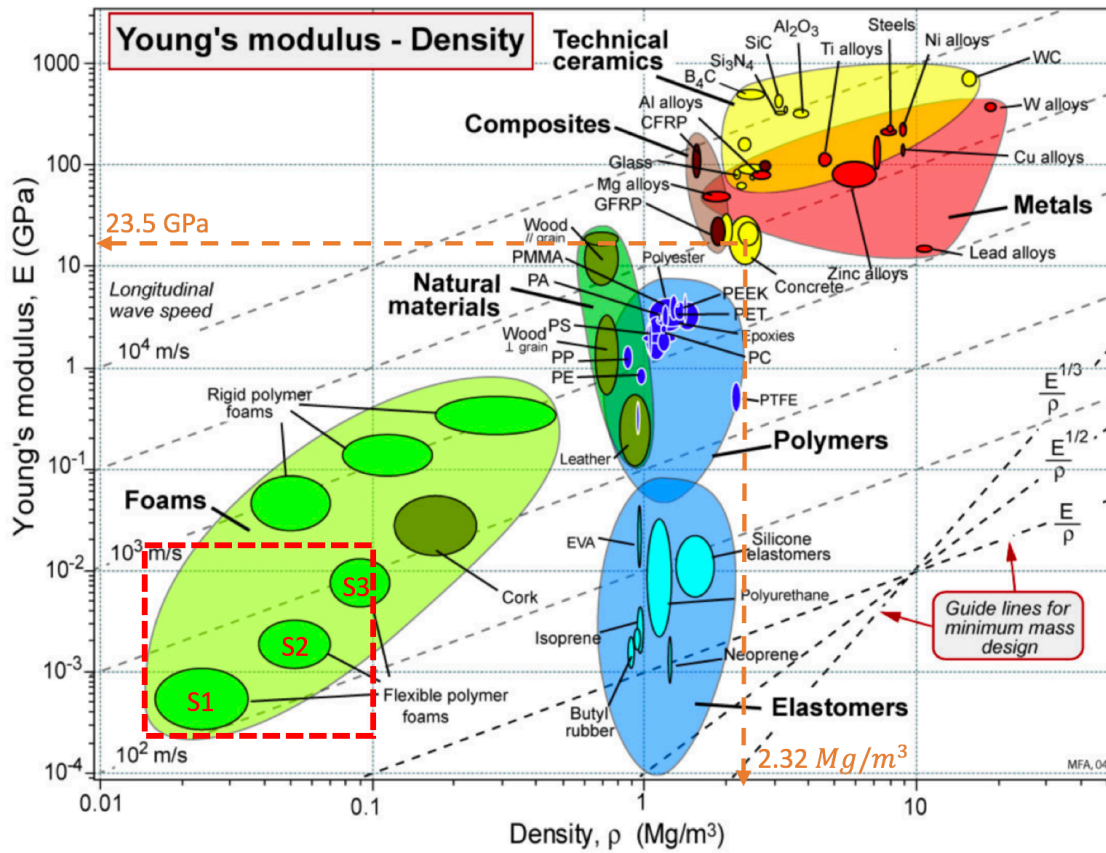
Figure 2.15 – The Young's modulus E and density ρ for the majority of the materials, reference from [1]

In the preceding discussion, the density contrast was found to have little impact on changing the cut-off frequency as compared with other parameters. For that reason, with respect to the contrast ratios, the contrast of mechanical property β_E should be paid more attention on as it is critical of determining the potential secondary material on the chart which will then lead to the position of the first cut-off frequency. Since the lowest stop band showed up, with regards to the gradient elasticity results elaborated afore, at β_E=0.001, the secondary material captured from figure 2.15 is in the sector of foams.

Here, the area of foams was enclosed by a red-dash square. As it can be noticed, there were three types of flexible polymer foams included in the square, distinctive to Young's modulus as well as density. Taking each type of these polymer foams and coupling with the primary material concrete, the combination with associated band gap can be found

in table 2.5. Note that, the materials given in figure 2.15 may be limited by options as compared with practical use, but they were worthwhile to take as a tangential solution to start with. Furthermore, the error tolerance in material properties had to be considered. In table 2.5, the cut-off frequencies were calculated based upon the averaged values of materials' properties.

Table 2.5 – The enclosed foam types coupled with concrete and associated cut-off frequencies resulted from each combination

Solution	Foam		Concrete		1st Cut-off Frequency/ Hz
	$E(GPa)$	$\rho(Mg/m^3)$	$E(GPa)$	$\rho(Mg/m^3)$	
S1	5×10^{-4}	0.025	23.5	2.32	5.47
S2	1.7×10^{-3}	0.050	23.5	2.32	10.05
S3	7×10^{-3}	0.090	23.5	2.32	20.60

Three combinations above have met the requirements for achieving desirable cut-off frequency level. In order to verify the performance of each combination, a numerical study was undertaken in section 3, in which the responses of the structure formed by the mentioned combination were obtained numerically, with careful settings in mesh and boundary conditions. The obtained results included the information about the ability of vibration attenuation.

It was also worth reminding the fact that the presence of stop band frequency was predicted by the elasticity gradient theory along with the definition of RVE in periodic structure. In this contribution, a unified gradient elasticity combining both statics and dynamics were employed in the formulation of mechanism. This unified gradient elasticity theory was highly recommended for not only its effective description in dispersive wave propagation, but also for the absence of complication of formulation and the consequent finite element implementation [80]. The simplicity of such a theory was due to the use of the RVE. With the illustration of equation 2.14, the gradient theory employed the homogenisation scheme which transformed a heterogeneous material into an effective homogeneous one. The main reason for using the second-order gradient theory was because of the automatic appearance of the length-scale parameter, which eased the transition of correlating the dimension of the RVE as presented in equation 2.15 and equation 2.16 [81].

3 NUMERICAL MODELLING

In this section, a one-dimensional finite element model was created in order to simulate the mechanisms of the structure as was imposed to the vibration forcing frequency. The methodology applied in building the model elements will be given in details in section 3.2. Results and discussion in section 3.4 were directed from the information observed from the numerical simulation. Moreover, a schematic diagram figure 3.17 was presented in section 3.3 for illustrating the pipeline of acquiring an optimal results for the purpose of this project, details being delivered in later sections.

3.1 Simulation method

To begin with, in the perspective of the theoretical concept, one could anticipates to observe stop band phenomena caused by the presence of heterogeneous material when the structure is exposed at certain frequency ranges, in which the vibration waves at all frequencies propagate themselves, following a similar behaviour [58]. According to section 1.2.3, the frequency range between 1-85 Hz was chosen to be the frequency domain of interest. Also, waves that are capable of propagating at all frequencies in this range are known as a passband. However, if waves failed in transmitting all frequencies (or partially transmit), the field that contains little propagation of waves is known as a stop band.

The finite element method was extensively used as a powerful tool in engineering studies. It builds mathematical models and provides numerical solutions for structures, particularly with complex geometry settings. For the intention of finding the structural performance issues, FEA models the product into virtual environment and solves differential equations that dictate the characteristics of the physical problem by discretising the whole structure into small mesh elements whose size and shape lead to the determination of solution's quantity and quality. In comparison to the analytical methods, FEA gained more reliability in predicting and improving the product's performance with feasible adjustments in all parameters. In addition, FEA is competent for analysing problems in cases of complex geometries as well as variations in timeframes. For that reason, FEA was selected to be more pronounced in performing the simulation.

A brief simulation procedure is given here in order to provide a systematic guidance in running the simulation.

1. selection of unknown state variables which describe the the system's behaviour when it is subjected to certain conditions

2. identification of mesh elements and integration to form a complete system

3. establishment of the system-governing equilibrium stated together with boundary conditions

4. collection of output results after running the simulations

3.2   One-dimensional finite element model

The structure of one-dimensional simulation model was presented in figure 3.16. Note that the figure presented here is not in scale. As it can be seen, the model comprised of four parts: $A1$, $A2$, B and C. While $A1$, $A2$ and B are symmetrical about C. The length of each part was given in the table 3.6. These parts were assumed to be perfectly bonded at the interfaces across which there is no discontinuity in displacements.
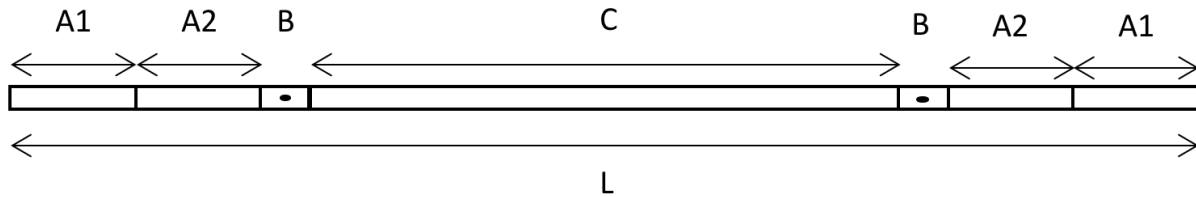
Figure 3.16 – The structure of one-dimensional simulation model.

Table 3.6 – The length of materials in the parts given in figure 3.16

Material	$A1$	$A2$	B	C
Length/mm	7500	7500	3000	15000

Although the simulation was formed with several material sections, part C was literally the section with the major concerns. The constitution of part C could be either of homogeneous or heterogeneous material, which depended on the modelling situations. Meanwhile, the arrangement of heterogeneous material in part C was organised in the form of either periodic (like what demonstrated in figure 2.4) or quasi-random. The selection of type of arrangement will be discussed thoroughly in the later section section 3.4.1. Parts B were designed to adhere on the ends of part C. The point in centre of

part B on the left acted as the vibration source and the point on the other part B was considered as a receiver point collecting the wave signals after propagation through part C. Part $A1$ and part $A2$ were perfectly matched layers (PMLs), which were attached to part B on both sides. The concept of PML will be explained in section 3.2.1.

3.2.1 Perfectly matched layers (PML)

The FEA model proceeds to a simulation with boundary conditions of having fixed ends, meaning that no displacements are allowed in neither direction. For a continuum mass structure subjected to dynamic loading, the vibration waves generally reflect no matter if there existing a transition from one material to another. These reflected waves can interference with the outgoing waves and create unwanted chaos, which potentially would result in a huge reduction in the accuracy of the output signal at the receiver point as well as the source point. To overcome this issue, perfectly matched layers (PMLs) were introduced as to place adjacent to the edges on both sides in order to absorb waves, and avoiding reflection from the interface.

As it can be seen in figure 3.16 from section 3.2, the PMLs presented here were $A1$ and $A2$. Part Bs being sections with the vibration source and the receiver point. In pursuance of creating perfectly matched layers, the impedance Z of the interface between part B and part $A2$ as well as part $A2$ and part $A1$ had to be equal to the same value. That is to say,

$$Z = Z_{B|A2} = Z_{A2|A1} \qquad \textbf{Equation 3.1}$$

This is because constant impedance allows waves to propagate without suffering from resistance so that no reflections will be produced at the interface. By making assumptions on the relation of the density and mechanical properties between materials, equation 3.1 can then be further written as

$$\sqrt{\rho_B \cdot E_B} = \sqrt{\rho_{A2} \cdot E_{A2}} = \sqrt{\rho_{A2} \cdot E_{A2}} \qquad \textbf{Equation 3.2}$$

where

$$\rho_{A1} = 50\rho_B \qquad\qquad E_{A1} = 0.02E_B$$
$$\rho_{A2} = 10\rho_B \qquad\qquad E_{A2} = 0.1E_B \qquad \textbf{Equation 3.3}$$

By doing so, a set of artificial absorbing layers, which are heavily lossy to incoming wave

pressure, were created. When a wave enters, it is attenuated by absorption and decays exponentially. Note that, to simplify the problem, the damping effect and Poisson's ratio of all materials were assumed to be zero.

3.2.2 Transmission coefficient

In the interest of appraising stop-band in a quantitative and qualitative way in the simulation, transmission coefficient T_c was chosen to evaluate the relative energy of wave transmission between the source and the receiver. For each test frequency, there were two simulations, one for heterogeneous materials and the other for homogeneous materials, undertaken as to obtain the displacements at the receiver point. The time-averaged amplitudes of displacements for both simulations were calculated as a consequence of employing fast Fourier transform. In this study, the transmission coefficient at a given test frequency was defined as the ratio of time-averaged amplitudes of heterogeneous material to that of homogeneous material, see equation 3.4.

$$T_c = \frac{A_{heter}}{A_{homo}}$$
Equation 3.4

Since the amplitudes of waves can be related to power, the transmission coefficient must, therefore, be less than or equal to 1 due to energy conservation. For the model operating at the assigned frequency range, the amplitudes obtained by heterogeneous material gradually decayed and dropped close to zero at certain frequencies, which led to the transmission coefficient being close to zero. As such, the attenuation mechanism of heterogeneous materials can be assessed in a full frequency domain, at the same time, the location of the presence of stop band, where T_c decreased to a value of less than 5%, and was determined and compared with the value predicted in section 2.

3.2.3 Newmark's method

Considering the validity of transmission the coefficient based upon the data of cumulative displacements at the receiver point, popular Newmark's method was employed to solve differential equations by numerical integration. The Newmark's procedure was expressed as the following equations:

$$\dot{u}_{n+1} = \dot{u}_n + (1 - \gamma) \cdot \Delta t \cdot \ddot{u}_n + \gamma \Delta t \cdot \ddot{u}_{n+1}$$
Equation 3.5

$$u_{n+1} = u_n + \Delta t \cdot \dot{u}_n + \frac{1 - 2\beta}{2} \cdot \Delta t^2 \cdot \ddot{u}_n + \beta \Delta t^2 \cdot \ddot{u}_{n+1} \qquad \textbf{Equation 3.6}$$

where u is displacement, $\dot{u}$ is velocity and $\ddot{u}$ is acceleration. Δt is the time step; γ and β are parameters that determine the accuracy as well as the stability of the integration. For the constant acceleration, $\gamma = 0.5$ and $\beta = 0.25$ resulted in an unconditionally stable integration.

3.2.4   Mass and stiffness matrix construction

The principle of assuring an accurate model performance was to produce an equilibrium energy state of the structure, under which the resultant force, due to stiffness and mass inertia, was balanced with the external load. Hence, understanding the implementation of stiffness and mass matrices for the proposed one-dimensional model played a critical role in the outcomes of simulation.

The one-dimensional model can be discretised into a series of elements with rectangular bar shapes, with each of them consistenting of two nodes. For continuum mechanics, the continuous displacement was given by **u** and the nodal displacement $\mathbf{d} = [d_{x1}, d_{x2}, d_{x3}, \dots]^T$. If the displacement was assumed to vary linearly, then

$$u(x) = a + bx \qquad \textbf{Equation 3.7}$$

where a and b are constant coefficients. Thereby, the shape function **N** can be defined by

$$\mathbf{N} = \begin{bmatrix} N_1 & N_2 \end{bmatrix} \qquad \textbf{Equation 3.8}$$

where

$$N_1 = (1 - \frac{x}{L_e}) \quad N_2 = \frac{x}{L_e} \qquad \textbf{Equation 3.9}$$

Therefore, $u(x) = \begin{bmatrix} N_1(x) & N_2(x) \end{bmatrix} (d_{x1} \quad d_{x2})^T$, which can be also read as $\mathbf{u} = \mathbf{Nd}$. Note that L_e is the length between two nodes in one element. The strain is given by

$$\begin{aligned} \varepsilon &= \frac{du(x)}{dx} \\ &= \frac{d}{dx} \begin{bmatrix} N_1(x) & N_2(x) \end{bmatrix} \begin{pmatrix} d_{x1} \\ d_{x2} \end{pmatrix} \\ &= \mathbf{LNd} \quad or \quad \mathbf{Bd} \end{aligned} \qquad \textbf{Equation 3.10}$$

where **L** is a modified derivative operator and **B** is the strain matrix. Their expressions were presented in equation 3.11 and equation 3.12 respectively.

$$\mathbf{L} = \begin{bmatrix} \frac{\partial}{\partial x} & 0 \\ 0 & \frac{\partial}{\partial y} \\ \frac{\partial}{\partial y} & \frac{\partial}{\partial x} \end{bmatrix}$$
Equation 3.11

However, for one-dimensional single degree of freedom, $\mathbf{L} = \frac{\partial}{\partial x}$. Therefore,

$$\mathbf{B} = \mathbf{LN} = \begin{bmatrix} \frac{dN_1(x)}{dx} & \frac{dN_2(x)}{dx} \end{bmatrix} \begin{pmatrix} u_1 \\ u_2 \end{pmatrix}$$
Equation 3.12

The minimum potential energy (Π) was given by subtracting the work done (W) by the external load p from the strain energy (U) stored in the body during deformation. Assuming there was no change in the in the total potential energy,

$$\delta\Pi = \delta U - \delta W = 0$$
Equation 3.13

While for continuum expression,

$$\delta\Pi = \int_\Omega (\delta\varepsilon)^T \cdot \sigma \cdot d\Omega - \int_\Omega (\delta u)^T \cdot p \cdot d\Omega = 0$$
Equation 3.14

$$\int_\Omega \left\{ (\mathbf{B} \cdot \delta\mathbf{d})^T \cdot E \cdot (\mathbf{Bd}) \right\} \cdot d\Omega - \int_\Omega (\mathbf{N} \cdot \delta\mathbf{d})^T \cdot p \cdot d\Omega = 0$$

$$(\delta\mathbf{d})^T \left(\int_\Omega \mathbf{B}^T \cdot E \cdot \mathbf{B} \cdot d\Omega \right) \mathbf{d} - (\delta\mathbf{d})^T \left(\int_\Omega \mathbf{N}^T \cdot p \cdot d\Omega \right) = 0$$

$$(\delta\mathbf{d})^T \left[\left(\int_\Omega \mathbf{B}^T \cdot E \cdot \mathbf{B} \cdot d\Omega \right) \mathbf{d} - \left(\int_\Omega \mathbf{N}^T \cdot p \cdot d\Omega \right) \right] = 0$$

$$since \quad \delta\mathbf{d} \neq 0$$

$$\left(\int_\Omega \mathbf{B}^T \cdot E \cdot \mathbf{B} \cdot d\Omega \right) \mathbf{d} - \left(\int_\Omega \mathbf{N}^T \cdot p \cdot d\Omega \right) = 0$$
Equation 3.15

$$Also \quad read \quad as \quad \mathbf{Kd} = \mathbf{F}$$

Where Ω is the volume domain and **N** and **B** are shape function and strain matrix defined

in equation 3.9 and equation 3.12 respectively. Hence, the stiffness matrix **K** is given by

$$\mathbf{K} = \int_{\Omega} \mathbf{B}^T \cdot E \cdot \mathbf{B} \cdot d\Omega \qquad \textbf{Equation 3.16}$$

And **F** includes the body force and external applied tractions.

$$\mathbf{F} = \int_{\Omega} \mathbf{N}^T \cdot p \cdot d\Omega \qquad \textbf{Equation 3.17}$$

The standard variational mass limping procedure was applied in order to find the formulation of the mass matrix. By taking kinetic energy as part of the governing equation, the equation yielded as equation 3.18, which included the element mass density ρ, the space that the volume occupied Ω as well as the moving velocity **v**.

$$T = \frac{1}{2} \cdot \int_{\Omega} \rho \cdot (\mathbf{v})^T \cdot \mathbf{v} \cdot d\Omega \qquad \textbf{Equation 3.18}$$

According to FEA's philosophy, the element velocity can be interpolated by incorporating it with the shape function which then leads to $\mathbf{v} = \mathbf{N} \cdot \dot{\mathbf{u}}$, in which **N** is a row vector for 1D cases and $\dot{\mathbf{u}}$ is a vector of nodal DOF velocities. Substituting it into equation 3.18 and the integral now becomes

$$T = \frac{1}{2} \cdot (\dot{\mathbf{u}})^T \cdot \int_{\Omega} \rho \cdot (\mathbf{N})^T \cdot \mathbf{N} \cdot d\Omega \cdot \dot{\mathbf{u}}$$

$$= \frac{1}{2} \cdot (\dot{\mathbf{u}})^T \cdot \mathbf{M} \cdot \dot{\mathbf{u}} \qquad \textbf{Equation 3.19}$$

Therefore, the formulation for mass matrix can be written as

$$\mathbf{M} = \int_{\Omega} \rho \cdot (\mathbf{N})^T \cdot \mathbf{N} \cdot d\Omega \qquad \textbf{Equation 3.20}$$

For further details in stiffness and mass matrices element values, please refer to appendix B.

3.2.5   Convergence study

In this section, the simulation model was undertaken by the process of numerical study which followed the principle of discretisation and solution of integrating the differential equations. The Newmark's method was incorporated to estimate the results of inter-

est, namely, displacements, velocities and accelerations. Therefore, *mesh element* size as well as *time step* size were considered to be critical in overlooking issues that significantly affect the accuracy. As a consequence, studies on convergence for both *mesh element* and *time step* were engaged at the phase of preliminary settings, prior to procuration of the transmission coefficient.

To begin with, in this study, the wave propagation was simulated by imposing a sinusoidal dynamic loading at the resource point. The mesh element size had to be, therefore, designed to seize the movement of wavelength at each test frequency. This suggested that the smallest wavelength determines the mesh element with which could be started. The wavelength expression was given in equation 3.21.

$$\lambda = \frac{V}{f}$$

Equation 3.21

Where f is the corresponding frequency, V is the wave speed, which reads as $V = \sqrt{E/\rho}$. If part C in figure 3.16 was assumed to be accounted for concrete uniformly ($E = 27.5GPa$ and $\rho = 2320kg/m^3$), then the elastic wave speed can be said to be 3442 m/s. The suggested element size has not exceeded one fifth of the smallest wavelength [83]. Thus, the maximum test frequency value comes with the minimum wavelength. According to equation 3.21, $\lambda_{min} = \sqrt{3342/85} = 6.27m$. As a result, the first attempt of mesh size was set to be $1m$ and the reduction iteration was undertaken until the error of recording results has less than 1% effect on the accuracy. The iteration table can be seen in table table 3.7.

The results showed that the convergent mesh element size was 100mm whose error was less than 1%.

Table 3.7 – The convergence study of mesh element size

Iteration	Mesh Size (mm)	Element Number	Recording Amplitude	Error
1	1000	NA	NA	NA
2	500	170	0.191842	-
3	250	340	0.192092	1.30%
4	**100**	842	0.193868	**0.92%**
5	50	1684	0.194058	0.098%

Similar to the procedure of acquiring mesh element size, the first reasonable time step

in Newmarks' formula was obtained by taking it 10 times smaller than the minimum time period of the wavelength. The equation of the time period for each test frequency is given by equation 3.22

$$T_\lambda = \frac{1}{f}$$

From which the minimum time period was estimated to be $T_\lambda = 1/85 = 0.0117s$ and thus, the initial time step for numerical integration was chosen to be $1.2 \times 10^{-3}s$. The results of time step convergence is shown in table 3.8. Time step of 1×10^{-3} was selected in the simulation according to its minimal error.

Table 3.8 – The convergence study of time step

Iteration	Time Step (s)	Recording Amplitude	Error
1	1.2×10^{-3}	0.194291	-
2	1×10^{-3}	0.194058	**1.02%**
3	5×10^{-4}	0.194036	0.01%
4	1×10^{-4}	0.194078	0.02%

Lastly, the convergence study assisted in deciding mesh element size as well as time step, which were of importance in the result's accuracy. The chosen element size and time step were 100 mm and 1×10^{-3}s respectively.

3.3   Overview of the procedure pipeline

In the section, an overview of the procedure pipeline shown in figure 3.17 was provided to demonstrate the key steps involved in this project. It seemed pertinent to summarise the preceding context and couple it with graphical illustration.
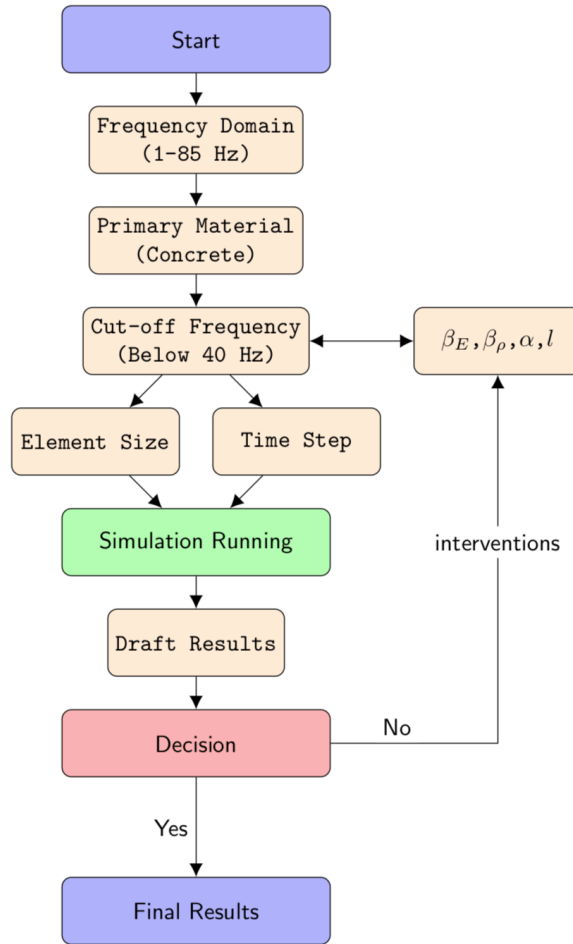
Figure 3.17 – The flowchart of the simulation process

In general, the project can be split into two major sections. The first section is known as material identification. According to the contents in aim and scope of section 1.3, a combination of two-phase heterogeneous material was desired to defined the vibration attenuation. This implied that the hostile frequency range was of a majority interest to the material selection because, with the primary material (concrete) remained constant, the secondary material with which the primary coupled would vary the stop bad frequency value that was predicted by the gradient elasticity theory. Furthermore, by altering the state variables in equation 2.30, the stop band frequency was reduced to an acceptable level, enabling an effective performance in numerical simulations to take place.

The second section came to model simulation in which the selected materials from the previous section were embedded into a one-dimensional single DOF structure. To ensure the quality and quantity of the simulation results, not only was the mathematical

model along with the integration method carefully constructed, but the element size and time step were also undertaken in the convergence study in order to minimise the error. The final conclusion can now be deduced after several interventions on state variables in equation 2.30.

3.4   Results and discussion

The purpose of this section was to verify the response of the modelled structure, by which the gradient elasticity theory was governed, as it was subjected to the dynamic loading conditions by demonstrating the mechanisms of the vibration wave dispersion along the length as they propagated. The following figure 3.18 showed the transmission coefficients recorded at the receiver point for different frequencies. The three sets of lines were the solutions proposed in table 2.5.
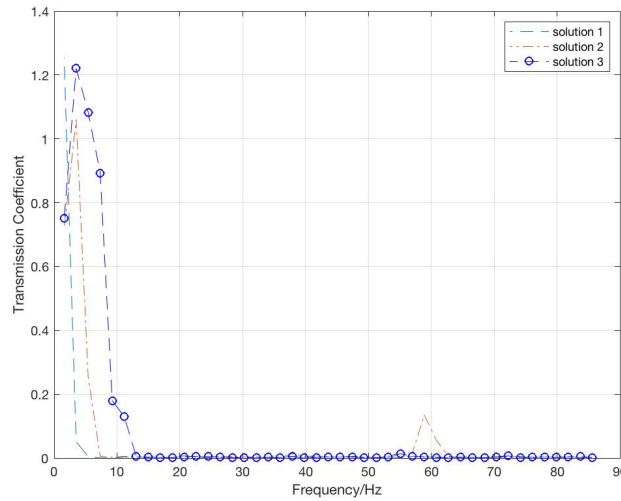
Figure 3.18 – The response of the three solutions proposed in table 2.5

The majority of the results were decreasing, except for solution 2, which illustrated a re-generation in T_c at 60 Hz. The solution 3 was taken in geometrical randomness analysis, however, the randomness effects produce a similar influence for the other two sets.

3.4.1   Addition of randomness in geometry

So far, the discussion was based on the heterogeneous material but was limited to a periodic arrangement. Also, the preceding section 2.5 has discovered that mechanical and

density contrast had a rather minimal effect on the stop-band structure of the composite in comparison with the geometrical length of the unit cell. Hence, to further improve the performance, it was of interest to introduce moderate perturbations to the geometry and observe its influence on the stop band as compared to the restricted periodic structure. Another reason for adding randomness in geometry in stead of mechanical and density was to avoid redefinition of materials.

In the context of this thesis, a methodology based on Fibonacci's sequence was employed in order to generate a geometrical disorder with controllable perturbations. The Fibonacci sequence based approach was recognised as a quasi- or pseudo-randomness because it offered a particular case of more generic randomness algorithm which could be manipulated by a user [2]. The graphical demonstrations of Fibonacci's layout of material with quasi-random properties can be found in appendix C.
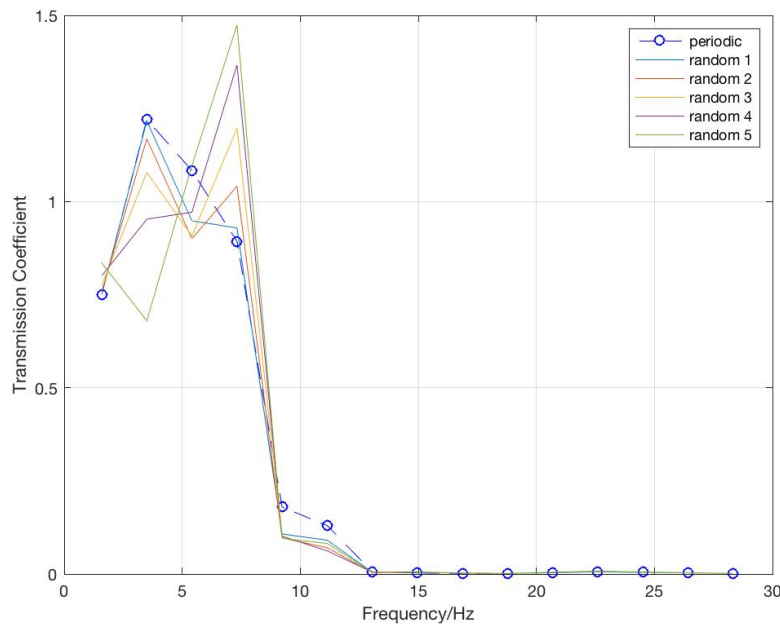
Figure 3.19 – The solution 3 with random geometry arrangements along the length

As it can be seen from the figure 3.19, a significant decrease in transmission coefficient was observed at the beginning of the wave propagation. The magnitudes started at approximately 1 and then dropped down to almost zero at the frequency value of 20Hz, which strongly agreed with the result predicted from elasticity gradient theory shown on table 2.5. By introducing randomness in structural geometry, there was no remarkable change in the position of the first stop band frequency. However, the picture de-

cayed with a higher rate in vicinity of the stop band frequency. In addition, the higher the randomness ratio is, the quicker the response decreases. The picture only demonstrated the patterns for frequency between 1 and 30 Hz, but there were little variation afterwards. Note that the picture have been averaged over 5 realisations of the simulation.

3.4.2 Discussion

It was clear to see that introducing randomness into the original periodic structure further reduced the amplitudes to lower frequencies, especially frequencies set just before the band gap. However, since the randomness only changed the arrangement of the adjacent cell but kept the length of the cell unchanged, the position of the first band gap was remained unaffected because the first stop band was directed with the value of the unit cell length [58], which was also reflected in equation 2.29 and equation 2.30. Although in some cases where the frequency range was large enough to capture a noticeable picture of pull-back in amplitudes which was so-called the second passband, it was not a primary objective of the present contribution as the frequency of interest was only limited from 1 to 85 Hz. The randomness in geometry with careful moderation will significantly translate the second passband into a stop band.

To attain the verification of band gap in frequencies, the transmission coefficient can be normally used as a useful reference. It simply measured the ratio of output and input. For transmission coefficient T_c approached zero, it implied that little wave propagation along the length, which indicated the occurrence of band gap. In order to present a better comparison in amplitude reductions, the input results was simulated by considering the whole model as an homogeneous material, whose properties corresponded to the harmonic mean of the Young's modulus and arithmetic mean of the density of the heterogenous material's properties (concrete and foam). Furthermore, part Bs of the model, which stood for the source and receiver, were chosen to be concrete. In this way, the transmission coefficient would below 1 if the output of heterogeneous' amplitudes was smaller than that of the homogeneous' amplitudes, meaning that heterogeneity would effectively create obstacles to the elastic wave propagation. On the other hand, in the context of this thesis, the simulation was attempting to offer a generic pattern of vibration reduction regardless of the magnitude of the external loading force. This external load would vary with a number of factors. For instance, the type of trains, the operating speed of the train, soil configurations in site and so forth. Therefore, the

transmission coefficient of the simulation for each frequency was thought to be an objective measurement compare to displacements at the testing point due to its nature of dimensionless. Although there were a few measured transmission coefficients greater than 1 antecedent to the first stop band frequency, the majority values agreed with the expectation that heterogeneous model resulted in a smaller displacement than the effective homogeneous model at a given frequency, in particular at higher frequencies. For those values of transmission coefficient greater than 1, the reasonable speculations were the absence of the effective homogeneous material in practice or the material was not classified as strain hardening material. The effective homogenised material had Young's modulus of $1.337 \times 10^{-4} GPa$ and mass density of $1.21 Mg/m^3$. This material was identified to be Elastomers according to figure 2.15 [1]. Hence, Elastomers would potentially return an unsteady responses when it was subjected to dynamic loading at various frequencies. An attempt that made to find an alternative homogenous material was to choose either concrete or foam which were used in the testing length. Nevertheless, the fundamental issue remained unsolved as neither concrete nor foam were strain hardening. In fact, they were both strain softening, thus they would lead to fluctuating patterns if they were considered to be the reference homogeneous material. In summary, the amplitudes of homogeneous material in the equation of transmission coefficient was decided to use the homogenised heterogenous of concrete and foam regardless of the unstable responses.

Furthermore, the rudimentary studies of both mesh element size convergence and time step convergence were scrutinised. The different element sizes and time steps were performed in the simulation. And they were finalised until the errors reduced within a acceptable range. Therefore, the studies were crucial in numerical simulations because they made the predicted results reliable.

4   CONCLUSION

The overall goal of this thesis was to reveal a proposition in the strategy that was implemented to reduce the ground-borne vibrations induced by the passage of high-speed trains. Inspired by the stop-band phenomena, the proposal of using heterogeneous material with periodic structural arrangements was numerically tested to be a potential approach when dealing with the excessive vibrations, thanks to their ability of stopping permittivity from propagation at certain frequency range which is dependent upon the material's properties.

Followed up with a systematic procedure derived from the elasticity gradient theory, the first stop band frequency was determined to the value desired by iterating the contrast ratios of material properties. It was discovered that geometrical contrast contributed the most significant effect on altering the stop band frequency value, followed by mechanical contrast, while, density contrast had little influence in comparison. However, the conclusion was phenomenological and was limited to the case in which the primary material was selected to be concrete. For different primary materials, the range of the contrast ratio may need to be redefined. The lowest stop band was found to occur at the highest contrast in Young's modulus ($\beta_E = 0.001$), at highest contrast in density ($\beta_\rho = 0.01$), and at the volume fraction to be 0.5. The identified material combination based on the findings above were concretes and foams. By increasing the unit cell length, it caused an exponential decrease in over stop band value. Therefore, a unit length of $3000mm$ was decided in this contribution, along with the parameters stated above.

The numerical simulation returned the results which strongly agreed with the stop band frequency predicted in the previous section. The transmission coefficient was used as a reference parameter which demonstrate the responses of the modelled structure when it was under the dynamic loadings. The adoption of transmission coefficient simplified the method while it provided generic and informative results. The absence of units in the transmission coefficient allowed it to be widely applied in other material combinations. However, the transmission coefficient would make more sense when the selected materials and their effective homogenised material were both strain hardening.

The quasi-randomness in material's geometry was studied by equipping the Fibonacci's sequences. Results showed that with increase in the randomness between two materials' geometrical length, the overall responses reduced quicker without altering the position of the stop band frequency value. Therefore, quasi-randomness can be used in order to improve the performance.

5 FUTURE PERSPECTIVE

In this thesis, in spite of the contributions have been made with regards to the proposal of a novel approach as to mitigate the ground-borne vibration induced by the passage of high-speed trains, the existence of technical difficulties remained challenging. Also, a desire for the need to further extend the study on both numerical and experimental model is a rather important issue to take into consideration for future works.

First and foremost, the mitigation strategy proposed in this thesis was to implement a sub-grading groove filled with heterogeneous materials arranged in controllable manner, so that the heterogeneity of the material would produce a stop band within the hostile frequency transmitted in the soil from the trains. This strategy requires such considerable capitals in construction as well as in a demand of large lands that investors are reluctant to consider it as an option in comparison with other existing techniques. Besides, an advanced technique in manufacturing a two-phase heterogeneous material is difficult and time consuming.

The numerical model designed in section 3 has only been performed in one-dimensional scenario. However, future studies may be demanded for extending the model into two- and three-dimensional applications. The numerical implementations and the associated analysis in situations of two- and three-dimensional models will open up new directions in this research, which encompasses the investigations of the sensitivity of quasi-randomness in materials's mechanical and geometrical properties. Structural damping effects and Poisson's ratio are needed for further explorations. Consequently, this higher dimensional model can be coupled with the soil ground model (mentioned in section 1.2.4) and together, they can produced a comprehensive simulation, which could possibly present the full-scale mechanisms of the vibration transmission.

It is frequently assumed that engineering drives the future in terms of establishing a society with sustainable developments and green infrastructures. A concern about the utilisation of waste and recycled materials in this mitigation strategy is conceivable. Possible future researches would need to be finding a pivot position as to maximise the effectiveness of material selections from a large diversity range without compromising the performance of the function of this vibration-proof strategy.

References

[1] **Mike Ashby**, "Material and process charts," Engineering Department, Cambridge CB2 1PZ, UK.

[2] **I.M. Gitman and Y. Song**, "Fibonacci sequence for modelling stop bands in random microstructure," *ZAMM Zeitschrift fur Angewandte Mathematik und Mechanik*, vol. 98, no. 2, pp. 270–276, October 2017.

[3] **Toolbox, Engineering**, "http://www.engineeringtoolbox.com/met-metabolic-rate-d_733.html," 2012.

[4] **Moshe Givoni**, "Development and impact of the modern high-speed train: A review," *Transport Reviews*, no. 26:5, pp. 1037–1061, 2007.

[5] **G. Kouroussis,O. Verlinden,C. Conti**, "Free field vibrations caused by high-speed lines: Measurement and time domain simulation," *Soil Dynamics and Earthquake Engineering*, no. 31, pp. 692–707, 2011.

[6] **David P. Connolly, Georges Kouroussis, Juliette Florentin, Calogero Conti, Olivier Verlinden**, "Building vibrations induced by railways: An analysis of commonly used evaluation standards," *The 21st International Congress on Sound and Vibration*, July 2014.

[7] **David P. Connolly, Grzegorz P. Marecki, Georges Kouroussis, Ioannis Thalassinakis, Peter K. Woodward**, "The growth of railway ground vibration problems — a review," *Science of the Total Environment*, no. 568, pp. 1276–1282, 2016.

[8] **L.Andersen and S.R.K.Nielsen**, "Reduction of ground vibration by means of barriers or soil improvement along a railway track reduction of ground vibration by means of barriers or soil improvement along a railway track," *Soil Dynamics and Earthquake Engineering*, no. 25, pp. 701–716, 2005.

[9] **G. Kouroussis,D.P. Connolly and O. Verlinden**, "Railway-induced ground vibrations – a review of vehicle effects," *International Journal of Rail Transportation*, vol. 2, no. 2, pp. 69–110, 2014.

[10] **D.P. Connolly, G. Kouroussis, O. Laghrouche, C.L. Ho and M.C. Forde**, "Benchmarking railway vibrations – track, vehicle, ground and building effects," *Construction and Building Materials*, vol. 92, pp. 64 − 81, 2015.

[11] **Sheng, X. and Jones, C.J.C. and Thompson, D.J.**, "A theoretical study on the influence of the track on train-induced ground vibration," *Journal of Sound and Vibration*, vol. 272, no. 3-5, pp. 909–936, 2004.

[12] **Veritchev, S.**, *Instability of a Vehicle Moving on an Elastic Structure.* DUP Science, 2002.

[13] **Connolly, D. P. and Kouroussis, G. and Laghrouche, O. and Ho, C. L. and Forde, M. C.**, "Benchmarking railway vibrations - Track, vehicle, ground and building effects," *Construction and Building Materials*, vol. 92, pp. 64–81, 2015.

[14] **Telford, William Murray and Geldart, L. P. and Sheriff, Robert E.**, *Applied Geophysics*, 1990.

[15] **Riccardo Ferrara, Giovanni Leonardi and Franck Jourdan**, "A two-dimensional numerical model to analyze the critical velocity of high speed infrastructure," *Fourteenth International Conference on Civil, Structural and Environmental Engineering Computing*, pp. 1–16, August 2013.

[16] **Fiala, P. and Gupta, S. and Degrande, G. and Augusztinovicz, F.**, "A parametric study on countermeasures to mitigate subway traffic induced vibration and noise in buildings," in *23rd International Conference on Noise and Vibration Engineering 2008, ISMA 2008*, vol. 5, 2008.

[17] **Lombaert, G. and Degrande, G. and François, S. and Thompson, D. J.**, "Ground-borne vibration due to railway traffic: A review of excitation mechanisms, prediction methods and mitigation measures," *Notes on Numerical Fluid Mechanics and Multidisciplinary Design*, vol. 126, pp. 253–287, 2015.

[18] **Thompson, David J**, *Railway Noise and Vibration. Mechanisms, Modelling and Means of Control*, 2009, vol. 53, no. 9.

[19] International Standards Organization, "ISO 2631-1: Mechanical Vibration and shock- Evaluation of human exposure to whole-body vibration- Part 1- General Requirements," 1997.

[20] International Standards Organisation, "ISO 2631-2: Mechanical vibration and shock – Evaluation of human exposure to whole-body vibration – Part 2- Vibration in buildings (1 Hz to 80 Hz)," 2003.

[21] **U. S. Department of Transportation (Federal Railroad Administration)**, *High-Speed Ground Transportation Noise and Vibration Impact Assessment*, 1998.

[22] International Standards Organisation, "ISO 14837-1:2005: Mechanical vibration — Ground-borne noise and vibration arising from rail systems — Part 1: General guidance," 2005.

[23] **Madshus, C. and Bessason, B. and Hårvik, L.**, "Prediction model for low frequency vibration from high speed railways on soft ground," *Journal of Sound and Vibration*, vol. 193, no. 1, pp. 195–203, 1996.

[24] **Thompson, D. J. and Jiang, J. and Toward, M. G.R. and Hussein, M. F.M. and Ntotsios, E. and Dijckmans, A. and Coulier, P. and Lombaert, G. and Degrande, G.**, "Reducing railway-induced ground-borne vibration by using open trenches and soft-filled barriers," *Soil Dynamics and Earthquake Engineering*, vol. 88, pp. 45–59, 2016.

[25] **Lamb, H.**, "On the Propagation of Tremors over the Surface of an Elastic Solid," *Philosophical Transactions of the Royal Society A: Mathematical, Physical and Engineering Sciences*, vol. 203, no. 359-371, pp. 1–42, 1904.

[26] **C. Y. Wang and J. D. Achenbach**, "Lamb's problem for solids of general anisotropy," *Wave Motion*, vol. 24, no. 3, pp. 227–242, 1996.

[27] **Salvador, Pablo and Real, Julia and Zamorano, Clara and Villanueva, Antonio**, "A procedure for the evaluation of vibrations induced by the passing of a train and its application to real railway traffic," *Mathematical and Computer Modelling*, vol. 53, no. 1-2, pp. 42–54, 2011.

[28] **Graves, Robert W.**, "Simulating seismic wave propagation in 3D elastic media using staggered-grid finite differences," *Bulletin of the Seismological Society of America*, vol. 86, no. 4, pp. 1091–1106, 1996.

[29] **Liu, G. R. and Quek, S. S.**, *The Finite Element Method: A Practical Course*, 2003.

[30] **Widas, Peter**, "Introduction to Finite Element Analysis," *Virginia Tech Material Science and Engineering*, no. January 2008, p. 87, 1997.

[31] **Smith, I M and Griffiths, D V**, "Programming the finite element method," p. 763, 1982.

[32] **Domínguez, J.**, *Boundary Elements in Dynamics*, 1993.

[33] **Çelebi, E. and Firat, S. and Çankaya, I.**, "The effectiveness of wave barriers on the dynamic stiffness coefficients of foundations using boundary element method," *Applied Mathematics and Computation*, vol. 180, no. 2, pp. 683–699, 2006.

[34] **Basu, Ushnish**, "Explicit finite element perfectly matched layer for transient three-dimensional elastic waves," *International Journal for Numerical Methods in Engineering*, vol. 77, no. 2, pp. 151–176, 2009.

[35] **Antonios Giannopoulos and S Melling and David Connolly**, "A second order pml implementation for fdtd seismic modelling," 9 2012.

[36] **Thornely-Taylor, Rupert**, "The prediction of vibration, groundborne and structure-radiated noise from railways using finite difference methods-part i-theory," vol. 26, 01 2004.

[37] **Katou, Masafumi and Matsuoka, Toshifumi and Yoshioka, Osamu and Sanada, Yoshinori and Miyoshi, Takayuki**, "Numerical simulation study of ground vibrations using forces from wheels of a running high-speed train," *Journal of Sound and Vibration*, vol. 318, no. 4-5, pp. 830–849, 2008.

[38] **Connolly, D. and Giannopoulos, A. and Forde, M. C.**, "Numerical modelling of ground borne vibrations from high speed rail lines on embankments," *Soil Dynamics and Earthquake Engineering*, vol. 46, pp. 13–19, 2013.

[39] **Connolly, D. and Giannopoulos, A. and Fan, W. and Woodward, P. K. and Forde, M. C.**, "Optimising low acoustic impedance back-fill material wave barrier dimensions to shield structures from ground borne high speed rail vibrations," *Construction and Building Materials*, vol. 44, pp. 557–564, 2013.

[40] **Ekevid, Torbjörn and Wiberg, Nils Erik**, "Wave propagation related to high-speed train a scaled boundary FE-approach for unbounded domains," *Computer Methods in Applied Mechanics and Engineering*, vol. 191, no. 36, pp. 3947–3964, 2002.

[41] **Galvín, P. and Domínguez, J.**, "Experimental and numerical analyses of vibrations induced by high-speed trains on the Córdoba-Málaga line," *Soil Dynamics and Earthquake Engineering*, vol. 29, no. 4, pp. 641–657, 2009.

[42] **Sheng, X. and Jones, C. J C and Thompson, D. J.**, "Prediction of ground vibration from trains using the wavenumber finite and boundary element methods," *Journal of Sound and Vibration*, vol. 293, no. 3-5, pp. 575–586, 2006.

[43] **C.J.C. Jones**, "Use of numerical models to determine the effectivenss of anti-vibration systems for railways," 1994. [Online]. Available: https://eprints.soton.ac.uk/157947/

[44] **Lutz Auersch**, "Mitigation of railway induced vibration at the track, in the www.elsevier.com/locate/procedia www.elsevier.com/locate/procedia x international conference on structural dynamics, eurodyn 2017 x international conference on structural dynamics, eurodyn 2017 mitigation of railway induced vibration at the track, in the transmission path through the soil and at the building," in *X International Conference on Structural Dynamics, EURODYN 2017*, vol. 199.   EURODYN 2017, 2017, pp. 2312–2317.

[45] **Nielsen, J. C.O. and Mirza, A. and Cervello, S. and Huber, P. and Müller, R. and Nelain, B. and Ruest, P.**, "Reducing train-induced ground-borne vibration by vehicle design and maintenance," *International Journal of Rail Transportation*, vol. 3, no. 1, pp. 17–39, 2015.

[46] **Faure, B. and Bongini, E. and Lombaert, G. and Guigou-Carter, C. and Herron, D.**, "Vibration mitigation by innovative low stiffness rail fastening systems for ballasted track," *Notes on Numerical Fluid Mechanics and Multidisciplinary Design*, vol. 126, pp. 627–634, 2015.

[47] **Coulier, Pieter and Hunt, Hugh E M**, "Experimental study of a stiff wave barrier in gelatine," *Soil Dynamics and Earthquake Engineering*, vol. 66, pp. 459–463, 2014.

[48] **Jones, C.J.C. and Thompson, D.J. and Andreu-Medina, J.I.**, "Initial theoretical study of reducing surface-propagating vibration from trains using earthworks close to the track," in *Proceedings of the 8th International Conference on Structural Dynamics, EURODYN 2011*, 2011.

[49] **Huston, D. R. and Johnson, C. C. and Wood, M. A. and Zhao, X.**, "Vibration attenuating characteristics of air filled seat cushions," *Journal of Sound and Vibration*, vol. 222, no. 2, pp. 333–340, 1999.

[50] **Çelebi, E. and Kirtel, O.**, "Non-linear 2-D FE modeling for prediction of screening performance of thin-walled trench barriers in mitigation of train-induced ground vibrations," *Construction and Building Materials*, vol. 42, pp. 122–131, 2013.

[51] **Yang, Yeong Bin and Hung, Hsiao Hui**, "A parametric study of wave barriers for reduction of train-induced vibrations," *International Journal for Numerical Methods in Engineering*, vol. 40, no. 20, pp. 3729–3747, 1997.

[52] **Adam, M. and Von Estorff, O.**, "Reduction of train-induced building vibrations by using open and filled trenches," *Computers and Structures*, vol. 83, no. 1, pp. 11–24, 2005.

[53] **Leung, K. L. and Vardoulakis, I. G. and Beskos, D. E. and Tassoulas, J. L.**, "Vibration isolation by trenches in continuously nonhomogeneous soil by the BEM," *Soil Dynamics and Earthquake Engineering*, vol. 10, no. 3, pp. 172–179, 1991.

[54] **Pieter Coulier, Geert Degrande, Arne Dijckmans, Jeroen Houbrechts, Geert Lombaert, Werner Rücker, Lutz Auersch, Miguel Rodríguez Plaza, Vicente Cuellar, David Thompson, Alf Ekblad, Alexander Smekal**, "Rivas wp 4.1 deliverable 4.1," in *SCOPE OF THE PARAMETRIC STUDY ON MITIGATION MEASURES ON THE TRANSMISSION PATH SCOPE OF THE PARAMETRIC STUDY ON MITIGATION MEASURES ON THE TRANSMISSION PATH*, 2011.

[55] **Adam, D and Vogel and Zimmermann**, "Ground improvement techniques beneath existing rail tracks," *Ground Improvement*, vol. 7621, no. 4, pp. 229–235, 2007.

[56] **Nawaz, Muhammad Farrakh and Bourrié, Guilhem and Trolard, Fabienne**, "Soil compaction impact and modelling. A review," *Agronomy for Sustainable Development*, vol. 33, no. 2, pp. 291–309, 2013.

[57] **Arulrajah, A. and Abdullah, A. and Bo, M. W. and Bouazza, A.**, "Ground improvement techniques for railway embankments," *Proceedings of the Institution of Civil Engineers - Ground Improvement*, vol. 162, no. 1, pp. 3–14, 2009.

[58] **Song, Yilang and Gitman, Inna M. and Parnell, William J. and Askes, Harm**, "The influence of random microstructure on wave propagation through heterogeneous media," *International Journal of Fracture*, vol. 204, no. 1, pp. 115–120, 2017.

[59] **Vasseur, J. O. and Djafari-Rouhani, B. and Dobrzynski, L. and Kushwaha, M. S. and Halevi, P.**, "Complete acoustic band gaps in periodic fibre reinforced com-

posite materials: The carbon/epoxy composite and some metallic systems," *Journal of Physics: Condensed Matter*, vol. 6, no. 42, pp. 8759–8770, 1994.

[60] **Kushwaha, M S and Halevi, P and Dobrzynski, L and Djafarirouhani, B**, "Acoustic Band-Structure of Periodic Elastic Composites," *Physical Review Letters*, vol. 71, no. 13, pp. 2022–2025, 1993.

[61] **J. D. Achenbach and M. Kitahara**, "Harmonic waves in a solid with a periodic distribution of spherical cavities," *The Journal of the Acoustical Society of America*, vol. 81, no. 3, pp. 595–598, 1987.

[62] **Liu, Zhengyou and Chan, C. and Sheng, Ping and Goertzen, A. and Page, J.**, "Elastic wave scattering by periodic structures of spherical objects: Theory and experiment," *Physical Review B - Condensed Matter and Materials Physics*, vol. 62, no. 4, pp. 2446–2457, 2000.

[63] **Vasseur, J. O. and Deymier, P. A. and Khelif, A. and Lambin, Ph and Djafari-Rouhani, B. and Akjouj, A. and Dobrzynski, L. and Fettouhi, N. and Zemmouri, J.**, "Phononic crystal with low filling fraction and absolute acoustic band gap in the audible frequency range: A theoretical and experimental study," *Physical Review E - Statistical Physics, Plasmas, Fluids, and Related Interdisciplinary Topics*, vol. 65, no. 5, p. 6, 2002.

[64] **Zhang, Shu and Hua, Jia and Cheng, Jian Chun**, "Experimental and theoretical evidence for the existence of broad forbidden gaps in the three-component composite," *Chinese Physics Letters*, vol. 20, no. 8, pp. 1303–1305, 2003.

[65] **Sigalas, M. M. and Economou, E. N.**, "Elastic and acoustic wave band structure," pp. 377–382, 1992.

[66] **Korringa, J**, "On the calculation of the energy of a Bloch wave in a metal," *Physica*, vol. 13, no. 6-7, pp. 392–400, 1947.

[67] **Kohn, W. and Rostoker, N.**, "Solution of the schrödinger equation in periodic lattices with an application to metallic lithium," *Physical Review*, vol. 94, no. 5, pp. 1111–1120, 1954.

[68] **Kafesaki, M. and Economou, E. N.**, "Multiple-scattering theory for three-dimensional periodic acoustic composites," *Physical Review B - Condensed Matter and Materials Physics*, vol. 60, no. 17, pp. 11 993–12 001, 1999.

[69] **Sigalas, M and Espinosa, F R Montero De and Torres, M and Kafesaki, M and García, N and Garcia-Pablos, D and Montero De Espinosa FR and Garcia, N**, "Theory and experiments on elastic band gaps," *Physical review letters*, vol. 84, no. 19, pp. 4349–52, 2000.

[70] **Tanaka, Y. and Tomoyasu, Y. and Tamura, S. I.**, "Band structure of acoustic waves in phononic lattices: Two-dimensional composites with large acoustic mismatch," *Physical Review B - Condensed Matter and Materials Physics*, vol. 62, no. 11, pp. 7387–7392, 2000.

[71] **Vasseur, J. O. and Deymier, P. A. and Chenni, B. and Djafari-Rouhani, B. and Dobrzynski, L. and Prevost, D.**, "Experimental and theoretical evidence for the existence of absolute acoustic band gaps in two-dimensional solid phononic crystals," *Physical Review Letters*, vol. 86, no. 14, pp. 3012–3015, 2001.

[72] **Aifantis, Elias C.**, "On the role of gradients in the localization of deformation and fracture," *International Journal of Engineering Science*, vol. 30, no. 10, pp. 1279–1299, 1992.

[73] **Liang Wu Cai and Shashidhar Patil**, "Effects of randomness on band gap formation in models of fiber-reinforced composite panels having quasirandom fiber arrangements," *Journal of Vibration and Acoustics*, vol. 129, no. 5, pp. 663–671, 2007.

[74] **Spencer, A.J.M.**, *Continuum Mechanics*, ser. Dover books on physics. Dover Publications, 2004.

[75] **Chong, Chi Ming**, "Experimental investigation and modeling of size effect in elasticity," Ph.D. dissertation, The Hong Kong University of Science and Technology, 2002.

[76] **Kouznetsova, V. and Geers, M. G.D. and Brekelmans, W. A.M.**, "Multi-scale constitutive modelling of heterogeneous materials with a gradient-enhanced computational homogenization scheme," *International Journal for Numerical Methods in Engineering*, vol. 54, no. 8, pp. 1235–1260, 2002.

[77] **Altan, B. S. and Aifantis, E. C.**, "On some aspects in the special theory of gradient elasticity," *Journal of the Mechanical Behavior of Materials*, vol. 8, no. 3, pp. 231–282, 1997.

[78] **Eringen, A. Cemal**, "On differential equations of nonlocal elasticity and solutions of screw dislocation and surface waves," *Journal of Applied Physics*, vol. 54, no. 9, pp. 4703–4710, 1983.

[79] **Askes, Harm and Metrikine, Andrei V.**, "Higher-order continua derived from discrete media: Continualisation aspects and boundary conditions," *International Journal of Solids and Structures*, vol. 42, no. 1, pp. 187–202, 2005.

[80] **Askes, Harm and Aifantis, Elias C.**, "Gradient elasticity in statics and dynamics: An overview of formulations, length scale identification procedures, finite element implementations and new results," *International Journal of Solids and Structures*, vol. 48, no. 13, pp. 1962–1990, 2011.

[81] **Gitman, Inna M. and Askes, Harm and Aifantis, Elias C.**, "The representative volume size in static and dynamic micro-macro transitions," *International Journal of Fracture*, vol. 135, no. 1-4, 2005.

[82] **Chen, W. and Fish, J.**, "A Dispersive Model for Wave Propagation in Periodic Heterogeneous Media Based on Homogenization With Multiple Spatial and Temporal Scales," *Journal of Applied Mechanics*, vol. 68, no. 2, pp. 153–161, 2000.

[83] **Marburg, Steffen**, "Discretization requirements: How many elements per wavelength are necessary?" in *Computational Acoustics of Noise Propagation in Fluids -Finite and Boundary Element Methods*, 2008, pp. 309–332.

A Codes for stop band prediction

```matlab
1  % This script offers a systematic approach to evaluate the first cut_off
2  % frequency value in heterogeneous structure from the associated parameters.
3  % The cut_off frequency prediction is formulated by the gradient thoery.
4  %
5  %
6  %   Essential parameters
7  % ========================
8  % - E1:             primary material' Young's modulus
9  %
10 % - rho1:          density of the primary material
11 %
12 % - beta_E:        mechanical property contrast ratio
13 %
14 % - beta_rho:      density contrast ratio
15 %
16 % - vf:            volume fraction of the periodic laminate
17 %
18 % - ls:            length of the periodic laminate
19 %
20 % Author: Zhan Zhang, Department of Mechanical Engineering, The University
21 % of Shefffield, ymiao1@sheffield.ac.uk, March 2018.
22 %=====================================================================
23 %%
24 clc; clear
25 % defining primary material properties
26 E1  =27500000;                      % primary material is concrete
27
28 rho1=2.32e-6;                       % concrete average density
29
30 beta_E=linspace(0.001,0.01,10);    % fraction of mechanical property
31
32 beta_rho=linspace(0.001,0.01,10);  % fraction of density
33
34 vf=linspace(0.1,1,10);             % volume fraction ratio
35
36 %% Mechanical property variation with beta_E and volume fraction
37 %=====================================================================
38 E=zeros(10);    % preallocating the matrix size
39 figure
```

```matlab
40  for i=1:10     % seting the row (beta_E) size = 10
41      for j=1:10 % column(volume fraction) size = 10
42          E(i,j)=E1 * beta_E(i)*E1 / ( (1-vf(j))*E1 + vf(j)*beta_E(i)*E1 ); ...
                % return the matrix of overall E, 10-by-10
43      end
44      plot(beta_E,E(i,:)); hold on                                        ...
            % plot the variation of E against vf for 10 different beta_E
45      %title('Youngs modulus variation with beta_E and vf')
46      xlabel('beta_{E}')
47      ylabel('Youngs modulus')
48      legendInfo{i}=['vf', num2str(i)]; % or whatever is appropriate
49      legend(legendInfo,'Location','northwest','Orientation','vertical')
50      axis([6e-3 9e-3 0 0.3e7])
51  end
52
53  %% Overall desnity variation with beta_rho and volume fraction
54  %=================================================================
55  rho=zeros(10); % preallocating the matrix
56  figure
57  for i=1:10     % beta_rho variation
58      for j=1:10 % volume fraction variation
59          rho(i,j) = vf(j) * rho1 + (1-vf(j)) * beta_rho(i)*rho1; % return ...
                the matrix of overall rho, 10-by-10
60      end
61      plot(beta_rho,rho(i,:)); hold on                        % plot ...
            the variation of rho against vf for 10 different beta_rho
62      %title('overall desnity variation with beta_rho and volume fraction')
63      xlabel('beta_{rho}')
64      ylabel('rho')
65      legendInfo{i}=['vf', num2str(i)]; % or whatever is appropriate
66      legend(legendInfo,'Location','northwest','Orientation','vertical')
67      axis([9e-3 10e-3 2.1e-6 2.35e-6])
68  end
69
70  %% Gama is a function of both beta_E and beta_rho, varying with vf, gamma ...
        = f ( beta_E, beta_rho, vf )
71  %=================================================================
72  gama=zeros([10 10 10]);% preallocating the matrix
73  figure
74  for i=1:10         % volume fraction range
75      for j=1:10     % beta_E range
76          for k=1:10 % beta_rho range
77  gama(i,j,k)=1/12 * ((vf(i)*(1-vf(i))*abs((E1*rho1 - ...
```

```matlab
              E1*rho1*beta_E(j)*beta_rho(k))))/...
78                  ((1-vf(i))*(vf(i) * rho1 + (1-vf(i)) * ...
                        beta_rho(k)*rho1)*E1+vf(i)*(vf(i) *...
79                      rho1 + (1-vf(i)) * beta_rho(k)*rho1)*E1*beta_E(j)))^2;
80              end
81          end
82  end
83
84  for i=1:10
85          surf(gama(:,:,i));hold on
86          xlabel('Beta E')
87          %xlim([0.001 0.01])
88          ylabel('Volume Fraction')
89          zlabel('gama ratio ')
90          axis ij
91          %set(plot,'LineStyle','none');
92          %colormap(jet)
93  end
94
95  %% Omega = f ( beta_E, beta_rho, vf, ls )
96  %===========================================
97  % this section is for calculating the cut off frequency range
98  clc;clear
99  E1 =2.33e7;             % primary material is concrete
100 rho1=2.32e-6;           % concrete average density
101 ls =3000;              % laminate size
102 beta_E=linspace(0.00001,0.001,10);   % fraction of mechanical property
103
104 beta_rho=linspace(0.01,1,10); % fraction of density
105
106
107 vf=linspace(0.1,1,10);               % volume fraction ratio
108
109 omega=zeros([10 10 10]);             % preallocating omega
110
111 for i=1:10
112      for j=1:10
113          for k=1:10
114
115          gama(i,j,k)=1/12 * ((vf(i)*(1-vf(i))*abs((E1*rho1 - ...
                    E1*rho1*beta_E(j)*beta_rho(k))))/...
116                  ((1-vf(i))*(vf(i) * rho1 + (1-vf(i)) * ...
                        beta_rho(k)*rho1)*E1+vf(i)*(vf(i) *  ...
```

```matlab
117                     rho1 + (1-vf(i)) * beta_rho(k)*rho1)*E1*beta_E(j)))^2;
118
119             E(i,j)=E1 * beta_E(j)*E1 / ( (1-vf(i))*E1 + vf(i)*beta_E(j)*E1);   ...
                    % overall E matrix
120
121             rho(i,k) = vf(i) * rho1 + (1-vf(i)) * beta_rho(k)*rho1;           ...
                    % overall density matrix
122
123             omega(i,j,k)=sqrt(E(i,j)/ls/ls/rho(i,k)/gama(i,j,k))/(2*pi);       ...
                    % first cut_off frequency
124
125         end
126     end
127 end
128
129 figure
130 for i=1:10 % 10 different density contrasts
131     surf(beta_E,vf,omega(:,:,i));hold on % hold on to stack them together
132     xlabel('beta E')
133     ylabel('Volume Fraction')
134     zlabel('Cut Off Frequency/ Hz ')
135     zlim([0 40])
136     %colormap(jet)
137     %set(gca,'xlim',[0 0.001])
138     %axis ij
139 end
140 %% this section is for quick calculations in the command window
141 %================================================================
142 % pre-defining the parameters
143 vf=0.1;
144 beta_E=0.01;
145 beta_rho=0.001;
146
147 gama_command=1/12 * ((vf*(1-vf)*abs((E1*rho1 - ...
        E1*rho1*beta_E*beta_rho)))/((1-vf)*(vf * rho1 + ...
148 (1                     -vf) * beta_rho*rho1)*E1+vf*(vf * rho1 + (1-vf) * ...
        beta_rho*rho1)*E1*beta_E))^2;
149
150 %% how does volume fraction affect the cut-off frequency given other ...
        factors remian the same
151 %================================================================
152 clc;clear
153 E1 =2.33e7;      % primary material is concrete
```

```matlab
154  rho1=2.32e-6;    % concrete average density
155  ls=3000;         % periodic length of the laminate
156  beta_E=0.001;    % mechanical property contrast
157  beta_rho=0.001;  % density contrast
158  vf=linspace(0.1,1,10); % 10 values of volume fraction from 0.1 to 1, ...
        interval 0.1
159
160  afg=zeros([10 1]);    % preallocating the vector
161  for i=1:10            % volume fraction variation
162      afg(i,:)=sqrt((E1 * E1*beta_E / ( (1-vf(i))*E1 + vf(i)*E1*beta_E ...
            ))/ls/ls/(vf(i) *...
163      rho1 + (1-vf(i)) * rho1*beta_rho)/(1/12 * ...
            ((vf(i)*(1-vf(i))*abs((E1*rho1 - E1*rho1*beta_E*beta_rho)))/...
164          ((1-vf(i))*(vf(i) * rho1 + (1-vf(i)) * ...
                beta_rho*rho1)*E1+vf(i)*(vf(i) * rho1 + ...
165          (1-vf(i)) * beta_rho*rho1)*E1*beta_E))^2));
166      afg(i,:)=afg(i,:)/2/pi;
167  end
168
169  figure
170  plot(vf,afg); grid on
171  xlabel('Volume Fraction')
172  ylabel('Cut Off Frequency/ Hz')
173
174
175  %% How does laminated cell length "ls" affect the cut-off frequency
176  %=====================================================================
177  % this section is for calculating the cut off frequency range
178  clc;clear
179  E1 =2.33e7;                      % primary material is concrete
180  rho1=2.32e-6;                    % concrete average density
181  ls=linspace(100,1500,10);       % laminate size
182  beta_E=linspace(0.00001,0.001,10);   % fraction of mechanical property
183
184  beta_rho=0.01;                   %linspace(0.001,0.01,10); % fraction of ...
        density
185
186  vf=linspace(0.1,1,10);           % volume fraction ratio
187
188  omega=zeros([10 10 10]);         % preallocating omega
189
190  for i=1:10
191      for j=1:10
```

```matlab
192            for k=1:10
193
194            gama(i,j)=1/12 * ((vf(i)*(1-vf(i))*abs((E1*rho1 - ...
                   E1*rho1*beta_E(j)*beta_rho)))/...
195                ((1-vf(i))*(vf(i) * rho1 + (1-vf(i)) * ...
                      beta_rho*rho1)*E1+vf(i)*(vf(i) * ...
196                rho1 + (1-vf(i)) * beta_rho*rho1)*E1*beta_E(j)))^2;
197
198            E(i,j)=E1 * beta_E(j)*E1 / ( (1-vf(i))*E1 + vf(i)*beta_E(j)*E1); ...
                   % overall E matrix
199
200            rho(i,:) = vf(i) * rho1 + (1-vf(i)) * beta_rho*rho1; ...
                            % overall density matrix
201
202            omega(i,j,k)=sqrt(E(i,j)/ls(k)/ls(k)/rho(i,:)/gama(i,j))/(2*pi); ...
                   % first cut_off frequency
203
204            end
205        end
206    end
207
208    figure
209    for i=1:10 % 10 different density contrasts
210        surf(beta_E,vf,omega(:,:,i));hold on % hold on to stack them together
211        xlabel('beta E')
212        ylabel('Volume Fraction')
213        zlabel('Cut Off Frequency/ Hz ')
214        zlim([0  40])
215        colormap(jet)
216        %axis ij
217        midpoint(i,:)=omega(end/2,1,i);
218    end
219
220    figure % how lowest cut-off frequency changes as cell length increases
221    plot(ls,midpoint','b--o')
222    grid on
223    xlabel('Cell Length/ mm')
224    ylabel('Cut Off Frequency/ Hz')
```

B Stiffness and mass matrix calculation

Recall the stiffness expression equation 3.16

$$\mathbf{K} = \int_{\Omega} \mathbf{B}^T \cdot E \cdot \mathbf{B} \cdot d\Omega$$

For linear shape variation, the shape function of each element was given by equation 3.9

$$N_1 = (1 - \frac{x}{L_e}) \quad N_2 = \frac{x}{L_e}$$

Since $\mathbf{L} = \frac{\partial}{\partial x}$, therefore, $\mathbf{LN}$ can be written as

$$\mathbf{LN} = \frac{\partial}{\partial x}[N_1 \quad N_2]$$

$$= \left[-\frac{1}{L_e} \quad \frac{1}{L_e}\right] \qquad \text{Equation B.1}$$

Meanwhile, $d\Omega = A_c \cdot dx.$, where A_c is the area of cross-section, which equals to 1 because the situation was restricted to one-dimension. The stiffness matrix $\mathbf{K}$ can now be expressed in the following form:

$$\mathbf{K} = \int_{\Omega} \mathbf{B}^T \cdot E \cdot \mathbf{B} \cdot d\Omega$$

$$= \int_0^{L_e} \left\{ \begin{bmatrix} -\frac{1}{L_e} \\ \frac{1}{L_e} \end{bmatrix} \cdot A_c \cdot E \cdot \left[-\frac{1}{L_e} \quad \frac{1}{L_e}\right] \right\} dx$$

$$= \frac{E}{L_e} \cdot \begin{bmatrix} 1 & -1 \\ -1 & 1 \end{bmatrix} \qquad \text{Equation B.2}$$

For mass matrix $\mathbf{M}$, recall equation 3.20

$$\mathbf{M} = \int_{\Omega} \rho \cdot (\mathbf{N})^T \cdot \mathbf{N} \cdot d\Omega$$

Therefore,

$$\mathbf{M} = \int_0^{L_e} \left\{ \rho \cdot A_c \cdot \begin{bmatrix} 1 - \frac{x}{L_e} \\ \frac{x}{L_e} \end{bmatrix} \cdot \left[1 - \frac{x}{L_e} \quad \frac{x}{L_e}\right] \right\} dx$$

$$= \frac{\rho L_e}{6} \cdot \begin{bmatrix} 2 & 1 \\ 1 & 2 \end{bmatrix} \qquad \text{Equation B.3}$$

C   Fibonacci layout of materials

The section provide the graphical demonstration of quasi-random geometries in the simulation model by incorporating the Fibonacci sequences. The Fibonacci sequences can be defined as $F^N = F^{N-1} + F^{N-2}$,with $N \geqslant 2$. The construction of the whole sequence depends on the first two seed values-F^1 and F^2. The Fibonacci bar consists of a series of cells. Each cell is formed of two materials differ in geometry, see figure 3.20.
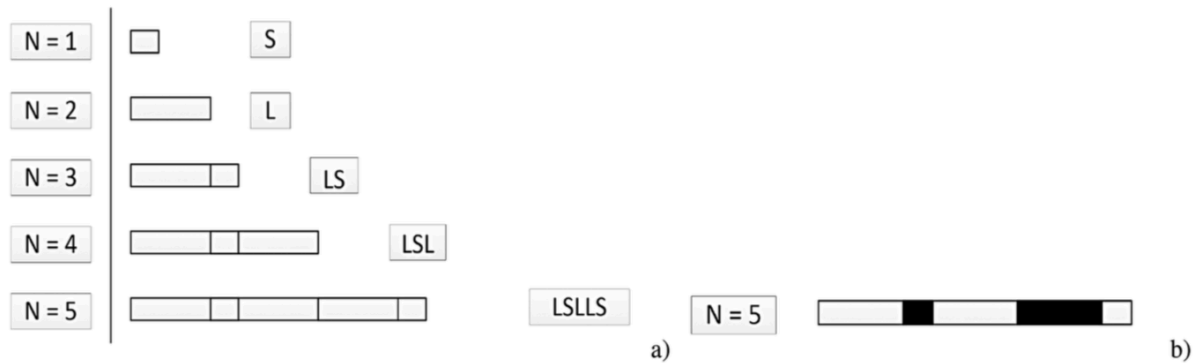
Figure 3.20 – Demonstrative picture of a Fibonacci bar construction, figure was credited from [2]

Note that S and L represented material's length. The starting seed values were chosen arbitrarily. If the starting values were equal in magnitude, the Fibonacci bar would be periodically constructed; if seed values are different, the arrangement of materials would close to random formation. The larger the difference between the starting values, the higher randomness rate.

The table below provided the information on the randomness construction for solution 3, shown in figure 3.19

Table 3.9 – The information on randomness applied in solution 3 in section 3.4.1

Randomness	F^1	F^2	N	Total Length
1	1500	1500	9	13500
2	1400	1600	9	13800
3	1300	1700	9	14100
4	1200	1800	9	14400
5	1100	1900	9	14700
6	1000	2000	9	15000